ENGINEERING DIVISION
U.S. ARMY ENGINEER REACTORS GROUP
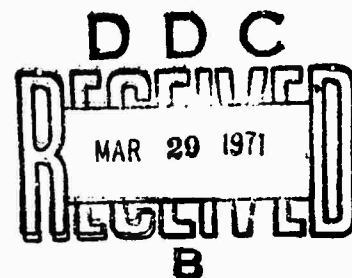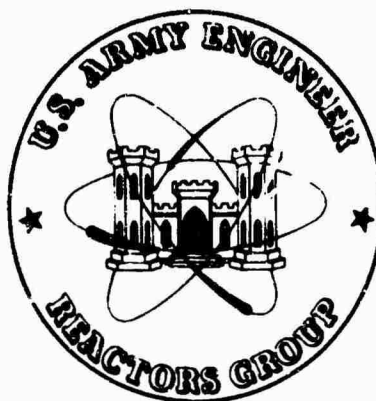**CORPS OF ENGINEERS**
FT. BELVOIR, VA. 22060

AD721019

ED-7102

THE THEORETICAL NUCLEAR ANALYSIS OF THE MH-1A:
CORES 2 AND 3

MICHAEL V. GREGORY
SHRINIVAS S. IYER
RICHARD A. LILLIE
C. DANIEL HENRY

1 MARCH 1971

D D C
RECEIVED
MAR 29 1971
B

Distribution of this document is unlimited

DISTRIBUTION STATEMENT A
Approved for public release;
Distribution Unlimited

110

The findings of this report are not to be construed as an official Department of the Army position, unless so designated by other authorized documents.

Destroy this report when it is no longer needed. Do not return it to the originator.

ED-7102

THE THEORETICAL NUCLEAR ANALYSIS OF THE MH-1A: CORES 2 AND 3

MICHAEL V. GREGORY
SHRINIVAS S. IYER
RICHARD A. LILLIE
C. DANIEL HENRY

1 MARCH 1971

ENGINEERING DIVISION
U. S. ARMY ENGINEER REACTORS GROUP
CORPS OF ENGINEERS

Distribution of this document is unlimited

ABSTRACT

This report presents the methods and results of the theoretical analysis of the nuclear properties of MH-1A Cores 2 and 3. The basic physical parameters are obtained by use of two cross-section codes, LEOPARD and LEOPROD, an X-Y geometry depletion code TURBO*, plus a Z-axial calculation using the CNCR-2 code together with the HOMOG and PEAK processor codes. The theory, results, and input details of the LEOPROD blackness theory code giving absorber region constants are considered in some detail.

TABLE OF CONTENTS

LIST OF TABLES

ii

LIST OF FIGURES

I. INTRODUCTION

A. Reactor and Power Plant Description

The MH-1A nuclear power plant is installed in a floating mount comprising a Liberty Ship hull, modified by the addition of a new mid-body. All of the original propulsion equipment has been removed, and the nuclear reactor and associated equipment have been located in the new mid-body. The Liberty Ship so modified has been named the "STURGIS".

The nuclear system is built around a 45-megawatt-thermal pressurized water reactor. The nuclear core utilizes low-enriched pellets of uranium dioxide in tubular fuel elements, boron steel control rods, and a single pass coolant flow.

The single reactor primary coolant loop and all associated equipment is housed in a containment vessel. Two canned rotor main coolant pumps mounted in parallel are required for reactor loop operation. The system pressurizer utilizes an electric heater and water quench system for maintaining proper pressure during operation. A vertical U tube steam generator is used to supply steam to the main turbine.

The electrical generating system generates the electricity required for plant operation as well as the 10 mw for external distribution. Either 50 or 60 cycle alternating current can be supplied (the 50-cps operation allows a maximum net output of 8.05 mw).

The power barge is operated by an all military crew of 68 men.

B. Facility Location

The MH-1A Floating Nuclear Power Plant (STURGIS) is designed to serve the United States Army as mobile source of power at any site accessible by waterways.

The STURGIS is presently moored in the northwest corner of Gatun Lake, approximately 1000 meters southwest of the city of Gatun, Panama Canal Zone, and approximately 250 meters northeast of the Gatun Hydroelectric Dam. The city of Gatun is located near the northwest (Caribbean) end of the Canal Zone.

1

C. The Analysis

This study presents the analysis performed to determine the behavior of MH-1A Core 2 and Core 3 (the second shuffle core).

The depletion study of the MH-1A shuffled core (the second core for this reactor) was performed using the TURBO* two-dimensional program. The cross-sections required for TURBO* (with the exception of control rod parameters) were obtained from the LEOPARD zero-dimensional code. An in-house modification of LEOPARD (named LEOPROD) was developed to calculate control rod constants based on blackness theory, and its output was used to provide the remaining input to TURBO*.

2

II. BACKGROUND

The MH-1A reactor is a pressurized light water cooled and moderated type utilizing stainless steel clad, low-enriched UO$_2$ fuel pellets. The core contains 32 fuel assemblies and 12 control rods, and is assembled to approximately a right circular cylinder with a fueled height of 36 inches and an equivalent diameter of 45.2 inches. The reactor is shown in Figure II-1, and the core arrangement in Figure II-2.

A. Type I Fuel Elements

The MH-1A reactor is fueled with low-enriched uranium dioxide incorporated into fuel elements. Each fuel assembly is made up of 104 fuel pins, each 39 inches long by 0.507 inch in diameter. The pins are formed of annealed tubes fabricated from type 348 stainless steel. These tubes are filled for 36 inches of their length with pellets made of uranium dioxide enriched to 4.65 weight percent in U-235. The tubes are filled with an inert atmosphere of helium.

The fuel loading is comprised of 32 of these fuel assemblies (designated as MH-1A Type I fuel elements) arranged in a square 6 x 6 array with corner elements missing. Two radial fuel zones are used with a refueling scheme employing fuel shuffling, both to increase fuel burnup and to improve core power distribution.

B. Refueling and Fuel Shuffling in MH-1A Type I Core

The outer 16 elements of the core are enriched to 4.65 percent in U-235 and the original inner elements were enriched to 4.07 percent in U-235. At the end of life of the original core (designated Core 1), the inner 16 elements were removed, the outer 16 elements were moved into the center, and 16 new elements enriched to 4.65 percent were added to the core outer region. This first shuffle core is designated Core 2. Subsequent shuffle cores are numbered sequentially.

C. Type I and Modified Type I Control Rods

There are 12 control rods, cruciform in cross section, which are used to start up and shut down the MH-1A reactor and to control the reactivity in the core while the reactor is operating. These control rods operate in channels among the fuel elements.

3

CONTROL ROD DRIVE
MECHANISM RACK
HOUSING

CONTROL ROD DRIVE
MECHANISM DRIVE
PACKAGE

LIFTING LUG
(4 PLACES)

SHIELD PLUG

SEAL LEAK BLEED LINE

DRAIN HOLE
(6 PLACES)

OUTLET NOZZLE

COVER PLATE

CORE-HOLDDOWN
STRUCTURE

CORE BARREL
ASSEMBLY

BORON 10

INLET NOZZLE

THERMAL SHIELDS

PRIMARY SOURCE
ROD ASSEMBLY

SHEATHING AND
INSULATION

PRESSURE VESSEL

ACTIVE
CORE
REGION

FUEL
ELEMENT

CORE SUPPORT
STRUCTURE

CONTROL ROD
ASSEMBLY

LOWER ORIFICE
PLATE

FIGURE II-1
REACTOR INTERNAL ARRANGEMENT
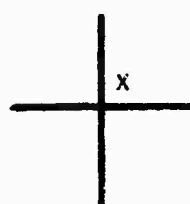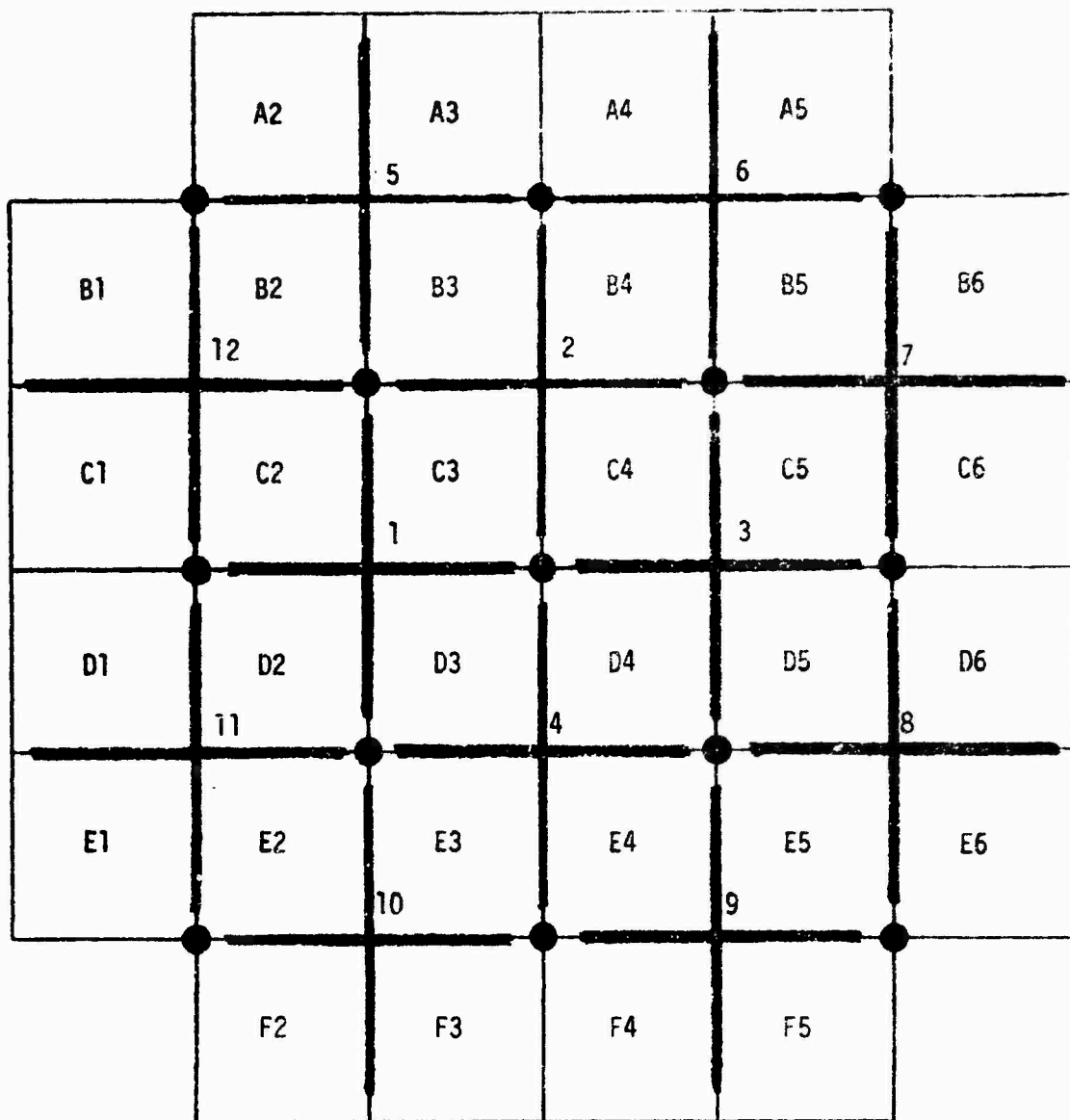
4
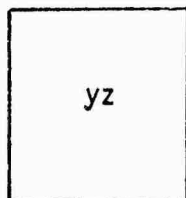
FIGURE II-2
CORE ARRANGEMENT

5

Type I control rods are boron stainless steel and have depletable followers. The rods consist of an upper highly absorbing control section containing 2.1 percent (by weight) boron-10 stainless steel encased in stainless steel cladding, with a follower section of slightly boronated stainless steel. The four inner control rods have followers of 0.16 weight percent natural boron equivalent in stainless steel; the eight outer ones have followers of 0.06 weight percent natural boron. The purpose of employing boronated followers was to assure that the one-rod shutdown criterion would be met and to flatten both the radial and axial power distributions.

Two sets of Type I control rods were obtained for use in the original core and the first three shuffle cores. The first set was to be used in the original core and the first shuffle core; the second, in the second and third shuffle cores. However, inspection of the first set of Type I control rods during the first shuffle of the core showed that cracks of undetermined cause existed in non-structural welds along the tips of some of the control rods. It was decided to use the second set in the first shuffle core. While it is expected that the second set of Type I control rods will perform better than the first set, due primarily to better quality control and inspection exercised during their manufacture, there is no assurance that similar cracks will not appear.

In order to assure that control rods are available for the operation of the second and third shuffle cores, new control rods have been ordered. These new control rods will have the lower borated follower plate replaced with a solid stainless steel plate since analysis has shown that shuffle cores can be operated safely with unborated followers. These control rods have been designated as Type I modified control rods.

D. Dummy Rod Locations

There are thirteen dummy rod locations in the MH-1A core. In the original core twelve of these locations (all but the center one) were filled with stainless steel dummy rods. The center dummy rod location was filled with a 0.507-inch diameter source element which consisted of a 6-inch long, 200 curie, PoBe source capsule at the core midplane with a 6-inch long, 0.14 weight percent natural boron-stainless steel poison slug below the source capsule.

In the first shuffle core the twelve stainless steel dummy rods were replaced by twelve 1.0 weight percent natural boron-stainless steel shim rods 0.507 inch in diameter. The source element was replaced by a new stainless steel dummy rod.

Table I gives the core design and characteristics.

6

TABLE I

CORE DESIGN AND CHARACTERISTICS

Plant Operating Data	
Thermal power in reactor (Mwth)	45
Electrical power produced,	
gross, 60 cycles (Mwe)	11.5
gross, 50 cycles (Mwe)	9.6
net, 60 cycles (Mwe)	10.0
net, 50 cycles (Mwe)	8.1
Core cycle lifetime (design), (yr)	1
Geometry	
Core configuration	6 x 6 w/corners missing
Active core hgt. (in.)	36.0
Equivalent dia. (in.)	45.2
Core Loadings	
Initial core - BOL	
Inner region (KgU)	1465 (4.07 w/o U-235)
Outer region (KgU)	1465 (4.65 w/o U-235)
Shuffled core - BOL	
Outer region (KgU)	1465 (4.65 w/o U-235)
Type I Fuel Elements	
Number of fuel pins per fuel element	104
Fuel pin pitch (in.)	0.654
Fuel pin OD (in.)	0.507
Active length (in.)	36

TABLE I (cont'd)

Total length (in.)	39
Fuel clad material	SS 348
Fuel clad thickness (in.)	0.023
UO_2 Pellet OD (in.)	0.4565
UO_2 Density (gm/cm^3)	10.35
Radial helium gap (cold)(in.)	0.00225

Type I Control Rods

Absorber

Shape	Cruciform
Blade width (in.)	
Inner 4 rods	10.78
Outer 8 rods	10.20
Absorber matrix composition	2.1 w/o B (92% B-10) in SS
Absorber thickness (in.)	0.250
Clad Material	SS 348
Clad thickness (in.)	0.050
Absorber length (in.)	36.75

Follower

Blade width (in.)	
Inner 4 rods	10.78
Outer 8 rods	10.20
Poisoned section length (in.)	27
Unpoisoned section length (in.)	14.9

TABLE I (cont'd)

Poison section composition	Nat. B in SS
Inner 4 rods (design)	0.16 w/o Nat B
Outer 8 rods (design)	0.06 w/o Nat B
Unpoisoned section composition	SS 348

Modified Type I Control Rods

Absorber

Shape	Cruciform
Blade width (in.)	
Inner 4 rods	10.78
Outer 8 rods	10.78
Absorber matrix composition	2.1 w/o B (92% B-10) in SS
Absorber thickness (in.)	0.250
Clad material	SS 347
Clad thickness (in.)	0.050
Absorber length (in.)	36.75

Follower

Blade width (in.)	
Inner 4 rods	10.78
Outer 8 rods	10.78
Total length (in.)	41.9
Composition	SS 347

Dummy Rods

Composition	Stainless Steel
Diameter (in.)	0.507

Shim Rods

Composition	1.0 w/o Nat. B - SS
Diameter (in.)	0.507

TABLE I (cont'd)

Source Rod	
Diameter (in.)	0.507
Source capsule:	
Length (in.)	6
Curies PoBe	200
Position	Core midplane
Poison Slug	
Length (in.)	6
Composition (w/o Nat B)	0.14
Position	Below Source Capsule

E. Summary of Analytical Procedures and Results

The analysis of a typical core proceeds in the following manner. First, the cross-sections for all regions in which the diffusion theory assumption of a slowly varying flux holds are obtained by the LEOPARD code as discussed in Section III. The regions in which diffusion theory is not valid, i. e., the absorber regions, are treated by the blackness theory formalism, and cross-sections for them are obtained by the LEOPROD code as discussed in Section IV.

Second, after all the cross-sections have been obtained, the two-dimensional (x-y) k calculations are performed by use of the TURBO* code. This code yields the appropriate k values for the two core temperatures (hot = 490°F, cold = 100°F; both average moderator temperatures) at both rods-in and rods-out configurations. Also, radial peaking factors are obtained from the x-y power distribution found by TURBO*. These procedures and results are discussed in parts of Sections V and VI.

Third, after the BOL radial calculations are completed, the axial calculations are performed. Using rods-in and rods-out TURBO* results, the HOMOG processor code yields average, homogenized constants for the axial calculations in which the core is represented as four regions: Top reflector, rodded region, unrodded region, and bottom reflector. These average constants are used in the CNCR-2 code which calculates the axial power distribution and k as a function of rod bank insertion. The results of CNCR-2 are analyzed by the PEAK processor code which yields the axial peak to average power plots. Sections V (J and K), and VI (D) discuss this aspect of the analysis.

The final step in analysis of a particular core is the depletion and life-time calculation. This is performed using the TURBO* program and its associated history tapes. Aspects of this analysis are discussed in Sections V and VI.

This report analyzes three core configurations. Based on earlier results for Core 1, the shuffle, reloading, and depletion of the resulting core (Core 2) are discussed in Sections V (A through D). After finding the end of life of Core 2 analytically, the shuffle and reloading resulting in Core 3 are discussed in the remainder of Section V. Due to the stuck rod results for Core 3, as discussed in Section VI (A), the analysis returned to Core 2 and depleted it further to 300 full power days. The core resulting from the subsequent shuffle and reloading, labelled Core 3A, is discussed in the remainder of Section VI.

Throughout the analysis, two different thermal group cross-section sets, the MND and the Wigner-Wilkens, are mentioned. The WW cross-section set results from assuming (as a model for thermalization) that the

moderator is a gas of hydrogen atoms exhibiting a Maxwellian distribution of velocities. This yields a tractable differential equation for the neutron spectrum in the thermal group. Averaging cross-sections over this neutron spectrum results in the WW thermal group cross-section set.

Alternatively, the neutron number density rather than the neutron flux may be used as the variable over which the spectrum is found. Averaging in this case results in the mixed number density (MND) cross-section set. Ordinarily the MND set is found by dividing the WW cross-sections by the spectrum averaged value of a 1/v absorber having unit cross-section at 2200 m/sec. Further discussion of the distinction between the two sets is presented in Section VI (B).

Table II summarizes some of the quantities found for the three cores.

<div align="center">TABLE II</div>

Comparison of Analytical Results for Cores 2,3, and 3A			
	Core 2	Core 3	Core 3A
BOL Loadings w/o U-235 (inner/outer)	4.22/4.65	4.35/4.65	4.28/4.65
Type of control rod follower	Borated SS	Borated SS/SS	SS
BOL k_{excess} hot cold	1.048 ---	1.058/1.091 1.123/1.155	1.086 1.152
Stuck rod shutdown margin	---	-1.22%/+0.21%	-1.899%
Radial peaking factor	1.68	1.83	1.92
Axial peaking factor	2.02	2.04	1.96
Core life (full power days)	253	---	395

III. UTILIZATION OF LEOPARD - FUEL, CLAD, AND MODERATOR CONSTANTS

LEOPARD (1) is a zero-dimensional code which calculates few group cross-sections for 35 elements throughout the spectrum changes resulting from depletion during core life. The fast group cross-sections are obtained by a 54-group MUFT calculation (a Fourier transform solution of the slowing down problem). The thermal group constants are calculated by a SOFOCATE code, yielding cross-sections averaged over a Wigner-Wilkins spectrum. From these Wigner-Wilkins values, the MND cross-sections are obtained through dividing by the spectrum averaged value of a 1/v absorber having unit cross-section at 2200 m/sec (LEOPARD actually takes one-sixth the spectrum averaged U-236 absorption cross-section; the U-236 absorption cross-section is 6.00 barns at 2200 m/sec).

Both the MUFT and SOFOCATE codes perform homogeneous calculations (i.e., there is no explicit representation of the fuel, void, clad, and moderator). The heterogeneities present in the physical reality are accounted for by modification of the homogeneous results through the calculation of the thermal utilization, resonance absorption, and the fast fission factor.

The MH-1A core consists of two different enrichment regions. At the beginning of core life the outer fuel elements are rotated inward and continue to be used in the shuffled core, while new 4.65 percent enriched elements are position as outer elements. Thus physically, slightly different flux characteristics are expected in the two different enrichment regions. This necessitates an approximation since only one set of cross-sections may be employed to describe the entire core during any particular time-step (i.e., the microscopic cross-sections which TURBO* uses for each type of atom is the same no matter where that type of atom is located in the core—in effect, a single flux energy-shape is assumed for the entire core for the purpose of obtaining cross-sections). Furthermore, the true composition of the rotated fuel elements is known only by calculation since the amount of real burn-up which each experienced while in the previous core cannot be measured physically.

To obtain these required parameters, the following steps were taken. The first core as loaded was known to have a nominal inner fuel element enrichment of 4.07 percent and a nominal outer fuel element enrichment of 4.65 percent. Thus, for the purpose of a LEOPARD calculation, the first core was represented as an averaged-core with average enrichment of 4.36 percent. Now, from the original-core TURBO* depletion study (Ref. 2), the calculated core life was 332 full power days. Hence, a LEOPARD depletion of the averaged-core was performed, using the same set of time steps as the TURBO* depletion, up to 332 full power days. This yielded an average core enrichment of 3.852 percent; that is, a

depletion of 0.508 percent during the course of core life. Since a uniform depletion of the core is assumed, the end of life enrichment of the outer elements is thus 4.142 percent (i.e., 4.65 percent minus 0.508 percent).

Thus the reshuffled core is represented as: New outer fuel elements of 4.65 percent enrichment, reused former outer elements as inner elements of 4.142 percent enrichment; the second averaged-core is thus represented by an average enrichment of 4.396 percent. The LEOPARD depletion of the shuffled core is performed for this averaged-core with the explicit representation of the trace elements (see Table III) carried in the reused fuel elements.

This type of averaging procedure is satisfactory for the LEOPARD cross-section generation since the cross-sections are relatively insensitive to the enrichment specified (i.e., the cross-sections for 4.142 percent enrichment differ only in the fourth digit from those for 4.65 percent enrichment). However, in the TURBO* calculation for the depleted core, all inner fuel element starting-number densities for depletable elements are taken from the final number densities resulting from the TURBO* depletion study of the original core (Ref 2).

The temperatures input into LEOPARD were based on the results of the CENTEM program (Ref 3), the calculations being for the half core presented in Figure 1. Table IV presents the results of these calculations.

For each fuel element, the temperature of clad and void $(\overline{T}_{c,v})$ is taken as: 1/2 (clad outer surface temperature) + 1/2 (fuel surface temperature). An all-core average is calculated by:

$$(\overline{T}_{c,v}) = \frac{2\,\overline{T}_{c,v}^{A} + 2\,\overline{T}_{c,v}^{B} + 2\,\overline{T}_{c,v}^{C} + \overline{T}_{c,v}^{D} + \overline{T}_{c,v}^{E}}{8}$$

where the superscript refers to the particular fuel element. This yields: $(\overline{T}_{c,v})$ = 615.8°F. An identical averaging process is used to obtain the core's volumetric average fuel temperature of 963.9°F. These temperatures are then used as input to the LEOPARD program, along with a moderator temperature of 490°F for the hot case and a resonance-effective temperature equal to the core volumetric average fuel temperature.

The parts of the LEOPARD output used in TURBO* consist of the cross-sections, self-shielding factors, and U-238 resonance escape probabilities at each depletion time-step, plus the starting number

14

densities (except as noted above for inner fuel elements). LEOPARD calculates the number densities of Pm-149 and I-135, but does not give the cross-section for these elements. Since both these elements are present in number densities of less than $10^{-8}/A^3$, these unavailable cross-sections may be neglected; and for the purposes of the TURBO* calculation, these elements will be considered absent in the core. On the other hand, although LEOPARD gives all the cross-sections and the number density for Pu-242, TURBO* does not have provision for this element. Again, since the number density of Pu-242 is $\geq 10^{-8}$, it may be considered absent. In any event, one has no choice but to omit these elements from the TURBO* calculations.

TABLE III

Trace Elements	
Element	Atoms/molecule of UO_2
U -236	1.0797×10^{-3}
Pu-239	2.1504×10^{-3}
Pu-240	1.3947×10^{-4}
Pu-241	2.6700×10^{-5}
Pu-242	7.1683×10^{-7}
Sm-149	4.0440×10^{-6}
Fission products	5.0247×10^{-3}

TABLE IV

CENTEM Results (Temps in °F)			
Fuel Element*	Fuel surface temp.	Clad outer surface temp.	Volumetric average fuel temp.
A	654.7	535.5	874.3
B	604.5	521.6	755.4
C	745.5	560.6	1112.8
D	695.8	546.8	978.4
E	792.1	573.4	1247.6

*see Figure III-1

16

FIGURE III-1

Half Core Used in CENTEM

A	B	
C	D	B
E	C	A
E	C	A
C	D	B
A	B	

Elements	Enrichment (w/o)
A, B	4.65%
C, D, E	4.142%

17

IV. CONTROL ROD CONSTANTS

A. _Theory_

Strictly speaking, the assumptions which lead to diffusion theory preclude the use of diffusion theory in regions where the flux undergoes abrupt changes, viz. in control rods. The approach of blackness theory (Ref 4, 5) is to define equivalent diffusion theory constants by treating these regions as isolated and applying the transport equation. Once these equivalent constants are found, the problem is wholly treated by the diffusion equation.

Four assumptions are made in the analysis:

1. No slowing down occurs in the absorber.
2. Scattering is neglected.
3. Diffusion theory is assumed to hold outside the region.
4. Absorption is only energy dependent (i.e., the region is homogeneous).

The absorbing region is taken to be a slab of thickness 2t. All quantities evaluated at the left face are denoted with a minus superscript, at the right face with a plus superscript.

The transport equation in the slab is:

$$\mu \frac{\partial \psi}{\partial Z} (Z, \mu, E) + \Sigma_a(E) \, \psi (Z, \mu, E) = 0$$

where $\psi (Z, \mu, E)$ is the directional flux, μ being the direction cosine. Henceforth, the energy argument E is understood.

For a neutron going from left to right (i.e., $0 < \mu \le 1$):

$$\psi^+ (\mu) = \psi^- (\mu) \exp [-2t \, \Sigma_a/\mu]$$

For a neutron going from right to left (i.e., $-1 \le \mu < 0$):

$$\psi^-(\mu) = \psi^+ (\mu) \exp [2t \, \Sigma_a/\mu].$$

From the P-1 solution to the transport equation:

$$\psi^- (\mu) = \phi^- + 3 \mu J^- \text{ for } 0 < \mu \le 1$$
$$\psi^+ (\mu) = \phi^+ + 3 \mu J^+ \text{ for } -1 \le \mu < 0$$

18

where ϕ is the scaler flux and J the current. Now $J^+ = 1/2\int_{-1}^1 d\mu \ \mu \ \psi^+ (\mu)$,

or $\quad J^+ = 1/2\int_{-1}^0 d\mu \ \mu[\phi^+ + 3\mu J^+] + 1/2\int_0^1 d\mu \ \mu \ [\phi^- + 3\mu J^-] \ \exp \ \underline{[-2t \ \Sigma_a]}$.

Define $E_{n+2} = \int_0^1 \mu^n \ e^{-T/\mu} \ d\mu$, the exponential integral(known as the "E functions"). Here $T = 2t \ \Sigma_a$, referred to traditionally as the "optical thickness".

Thus,

$$J^+ = -1/2 \ \phi^+ + E_3 \ (T) \ \phi^- + 3E_4 \ (T) \ J^-$$
$$J^- + 1/2 \ \phi^- - E_3 \ (T) \ \phi^+ + 3E_4 \ (T) \ J^+$$

(Note, to preclude confusion, that E without a subscript is simply the energy argument, while E_n with a subscript n is the E-function of type n).

Now, define the blackness coefficients:

$$\alpha(E) = \frac{J^-(E) - J^+(E)}{\phi^-(E) + \phi^+(E)} = \frac{1 - 2E_3(T)}{2(1 + 3E_4(T))}$$

$$\beta(E) = \frac{J^-(E) + J^+(E)}{\phi^-(E) - \phi^+(E)} = \frac{1 + 2E_3(T)}{2(1 - 3E_4(T))}$$

where the optical thickness T is a function of energy since Σ_a is a function of energy. The α and β definitions may be employed in the transmission matrix form (2):

$$\alpha \ (\phi^- + \phi^+) = J^- - J^+$$

$$\beta \ (\phi^- - \phi^+) = J^- + J^+$$

or

$$\begin{pmatrix} \phi^- \\ J^- \end{pmatrix} = \begin{pmatrix} \dfrac{\alpha + \beta}{\beta - \alpha} & \dfrac{2}{\beta - \alpha} \\ \dfrac{2\alpha\beta}{\beta - \alpha} & \dfrac{\alpha + \beta}{\beta - \alpha} \end{pmatrix} \begin{pmatrix} \phi^+ \\ J^+ \end{pmatrix}$$

19

For this geometry, the transmission matrix M is known (Ref 5):

$$\begin{pmatrix} \phi^- \\ J^- \end{pmatrix} = (M) \begin{pmatrix} \phi^+ \\ J^+ \end{pmatrix}$$

where

$$\left(M \right) = \begin{pmatrix} \cosh \dfrac{2t}{L} & \dfrac{L}{D} \sinh \dfrac{2t}{L} \\[2em] \dfrac{D}{L} \sinh \dfrac{2t}{L} & \cosh \dfrac{2t}{L} \end{pmatrix}$$

Equating the quotients of the off-diagonal terms, one obtains:

$$\alpha(E)\,\beta(E) = \left[\frac{D(E)}{L(E)}\right]^2 = D(E)\,\Sigma_a(E).$$

Equating the quotients of the second column entries, one obtains:

$$\frac{2}{\alpha(E) + \beta(E)} = \frac{L(E)}{D(E)} \tanh \frac{2t}{L(E)} \qquad \frac{2\sqrt{\alpha(E)\beta(E)}}{\alpha(E)+\beta(E)} = \tanh \frac{2t}{L(E)}.$$

Thus
$$\frac{2t}{L(E)} = \tanh^{-1} \frac{2\sqrt{\alpha(E)\beta(E)}}{\alpha(E) + \beta(E)} = \ln \frac{\sqrt{\beta(E)} + \sqrt{\alpha(E)}}{\sqrt{\beta(E)} - \sqrt{\alpha(E)}}$$

Now,
$$\frac{1}{L(E)} = \frac{\Sigma_a(E)}{\sqrt{D(E)}}$$

thus
$$\frac{\sqrt{\Sigma_a(E)D(E)}}{L(E)} = \Sigma_a(E) = \frac{\sqrt{\alpha(E)\beta(E)}}{2t} \ln \frac{\sqrt{\beta(E)} + \sqrt{\alpha(E)}}{\sqrt{\beta(E)} - \sqrt{\alpha(E)}}$$

$$D(E) = \frac{\alpha(E)\beta(E)}{\Sigma_a(E)} = \frac{2t\sqrt{\alpha(E)\beta(E)}}{\ln \dfrac{\sqrt{\beta(E)} + \sqrt{\alpha(E)}}{\sqrt{\beta(E)} - \sqrt{\alpha(E)}}}$$

Thus the equivalent Σ_a and D may be found for the region purely in terms of true region thickness, and α and β which depend solely upon the optical thickness.

20

The above development is for the case of a continuous energy model. An entirely equivalent result is obtained when the analysis is extended to group theory (Ref 4). In that case α and β are simply replaced by $\langle\alpha\rangle_n$ and $\langle\beta\rangle_n$ which are defined as appropriate average values of $\alpha(E)$ and $\beta(E)$ over the energy interval making up group n. Once $\langle\alpha\rangle_n$ and $\langle\beta\rangle_n$ are obtained, a calculation identical to those made above is made to obtain the group constants D_n and $\Sigma_{a,n}$.

The above formalism is developed for the case of continuous media. However, in reality most calculations are made with a finite difference approximation representing the spatial derivatives of the diffusion equation. This makes the value for the equivalent diffusion theory constants dependent upon the mesh spacing chosen in solving the finite difference equations. It can be shown (Ref 4) that the resulting expressions in that case are:

$$k_n = 1/2t \; \cosh^{-1} \; \frac{\langle\beta\rangle_n + \langle\beta\rangle_n}{\langle\beta\rangle_n - \langle\alpha\rangle_n}$$

$$D_n = \frac{(\langle\alpha\rangle_n + \langle\beta\rangle_n)h}{2 \sinh k_n h} \; \tanh \; 2k_n t$$

$$\Sigma_{a,n} = \frac{2 \, D_n}{h^2} \; (\cosh k_n h - 1)$$

where h is the mesh spacing and 2t the absorber slab thickness. As expected when $h \rightarrow o$, the continuous media expressions are recovered.

For the case where the mesh spacing is chosen to be one-half the slab thickness (i.e., there is only one mesh point midway in the slab and mesh points at each surface of the slab), namely $h = t$, then simpler equations result (Ref 6):

$$D_n = h \; \sqrt{\langle\beta\rangle_n \; (\langle\beta\rangle_n - \langle\alpha\rangle_n)}$$

$$\Sigma_{a,n} = \frac{2}{h} \; (\langle\beta\rangle_n - \sqrt{\langle\beta\rangle_n \; (\langle\beta\rangle_n - \langle\alpha\rangle_n)})$$

B. Application

LEOPROD, an in-house modification of the LEOPARD code (Ref 1), was used to generate the equivalent diffusion theory constants for the control rods. The usual LEOPARD spectrum-averaging procedures used to obtain group absorption cross-sections in the unit fuel cell were modified to calculate the $\langle\alpha\rangle_n$ and $\langle\beta\rangle_n$ in three fast groups and one thermal group.

21

The thermal spectrum averaged values were obtained using the Wigner-Wilkins spectrum generated by LEOPARD for the particular fuel cell. Values for the E_2 function are entered in tabular form through DATA statements for 46 values of the argument ranging from 0.0 to 22.0 (for > 22, $E_2 < 10^{-11}$ and hence is taken as zero). LEOPROD then creates tables of the E_3 and E_4 functions for the same 46 arguments using the recursion relations:

$$E_3(T) = 1/2 \ [e^{-T} - T * E_2(T)]$$

$$E_4(T) = 1/3 \ [e^{-T} - T * E_3(T)].$$

The number densities of boron-10, iron, nickel, chromium, and manganese are entered as input, and LEOPROD calculates the optical thickness T for the case by summing the macroscopic cross-sections contributed by each element at the energy of interest. The parabolic interpolation function TERP is retained from LEOPARD and used to calculate values of $E_3(T)$ and $E_4(T)$ different from the tabulated list. From these values of E_3 and E_4, values of $<\alpha>_n$ and $<\beta>_n$ for $1 \leq n \leq 172$ are calculated. These values for the 172 thermal subgroups are then averaged to obtain a thermal group average value by the following quadrature formula:

$$
<\alpha>_{th} = \left\{ \sum_{\ell=1}^{171} (W_\ell <\alpha>_\ell \sqrt{E_\ell} + W_{\ell-1} <\alpha>_{\ell-1} \sqrt{E_{\ell-1}}) \ (E_\ell - E_{\ell-1}) \right.
$$

$$
+ \ [W_{171} \ \sqrt{E_{171}} \ <\alpha>_{171} + \left(\frac{E_{max} - E_{171}}{E_{172} - E_{171}}\right)\left(W_{172} \ \sqrt{E} \ <\alpha>_{172} - \right.
$$

$$
\left. W_{171}\sqrt{E_{171}} \ <\alpha>_{171}\right) + W_{171} \ \sqrt{E_{171}} \ <\alpha>_{171}\Big] \ (E_{max} - E_{171}) \right\} * \left\{ \sum_{\ell=1}^{171} \right.
$$

$$
(W_\ell \sqrt{E_\ell} + W_{\ell-1} \ \sqrt{E_{\ell-1}}) \ (E_\ell - E_{\ell-1}) + [W_{171} \ \sqrt{E_{171}} + \left(\frac{E_{max} - E_{171}}{E_{172} - E_{171}}\right)(W_{172}\sqrt{E_{172}}
$$

$$
\left. - W_{172} \ \sqrt{E_{171}}) + W_{171} \ \sqrt{E_{171}} \ \Big] \ (E_{max} - E_{171}) \right\}^{-1}
$$

where E_ℓ is the average energy of the ℓ-th energy subgroup (not the E_ℓ function !!), the W_ℓ are the weight factors for each subgroup, and E_{max} the thermal cut-off (0.625 ev). An identical equation holds for $<\beta>_{th}$ with $<\alpha>_\ell$ replaced by $<\beta>_\ell$.

The fast spectrum averaging proceeds in an analogous manner with 54 fast subgroups (subgroups 1 through 10 being the first fast group, 10 Mev to 821 kev; subgroups 11 through 25 being the second fast group, 821 kev to 5.52 kev; subgroups 26 through 54 being the third fast group, 5.53 kev to 0.626 ev). Thus 54 values of $<\alpha>_\ell$ and $<\xi>_\ell$ are calculated in the same manner as for the thermal subgroups.

The averaging procedures is slightly different than that employed in the thermal group. Again as quadrature formula is employed:

$$<\alpha>_n = \frac{\displaystyle\sum_{\ell=1}^{j} <\alpha>_\ell\, \gamma_\ell/(1 + \sqrt{3}\, <\alpha>_\ell)}{\displaystyle\sum_{\ell=i}^{j} \gamma_\ell/(1 + \sqrt{3}\, <\alpha>_\ell)}$$

where the i and j limits define the group; that is,

$1 \le \ell \le 10$ for group 1, n = 1

$11 \le \ell \le 25$ for group 2, n = 2

$26 \le \ell \le 54$ for group 3, n = 3.

An identical procedure is used in obtaining $<\xi>_n$. The γ_ℓ represent the weight factor for the ℓ subgroups. This quadrature scheme differs from that used for the thermal group in the $\dfrac{1}{1 + \sqrt{3}\, <\alpha>_\ell}$ and $\dfrac{1}{1 + \sqrt{3}\, <\xi>_\ell}$ factors present. These factors are derived from the narrow resonance approximation (Ref 6) and account for the flux dip at the surface of the rod.

The input to the LEOPROD program is identical to that for LEOPARD (as used in the no burn-up option) with one exception. An additional data card is added after the card indicating the LEOPARD options chosen. This additional card is punched in six fields of twelve columns: The first being the boron-10 number density; the second, the slab thickness (in centimeters); the third, the iron number density; the fourth, the nickel number density; the fifth, the chromium number density; the sixth, the manganese number density. All number densities are in terms of atoms per cm^3 times 10^{24}.

The program may be adapted for absorbers other than boron-10, as long as they exhibit a 1/v absorption behavior (e.g., europium). In that case it is necessary to enter an equivalent boron-10 number density:

$$\left\{\begin{array}{l}\text{equivalent boron-10}\\ \text{number density}\end{array}\right\} = \left(\frac{\sigma_\alpha \text{ of absorber X at 2200 m/sec}}{\sigma_\alpha \text{ of boron-10 at 2200 m/sec}}\right)\left(\begin{array}{l}\text{absorber X}\\ \text{number density}\end{array}\right)$$

23

Of course, only the thermal group constants (where the 1/v relation holds) will have meaning. The fast group constants will not be correct unless, fortuitously, the fast absorption characteristics of absorber X are just the above conversion factor times the boron-10 fast absorption characteristics, with exactly parallel resonances. In any event, absorption in the thermal group is significantly greater than in the fast groups and, as a first approximation, one might accept the resulting fast group constants as roughly proper for absorber X.

The output is modified somewhat from that of the original LEOPARD output. Essentially, the first two pages of a LEOPARD output are retained since they provide a check of the input quantities for possible errors. The third page presents the output unique to the LEOPARD program: Number densities in the control rod, rod thickness, and blackness theory results. Both Wigner-Wilkins and MND results are presented for the thermal group. The MND results are obtained by dividing $\langle\alpha\rangle_{th}$ and $\langle\beta\rangle_{th}$ resulting from the Wigner-Wilkins spectrum calculation by the spectrum average value of a 1/v absorber having unit cross-section at 2200 meters/second. This average value is denoted by "Wigner-Wilkins 1/v" in the standard LEOPARD output. (For additional description of LEOPROD, refer to Section VII of this report.)

C. Results

The results obtained from the LEOPROD program are discussed in this section. Table V compares the blackness theory parameters $\langle\alpha\rangle_n$ and $\langle\beta\rangle_n$ obtained by the LEOPROD program to those obtained by NUS (Ref 7) which also used blackness theory for identical control rods but obtained spectra from the KATE and THERMOS codes. The agreement for the thermal group is precise. There is good agreement of these parameters for groups two and three; however, discrepancies appear in the group one results. It should be pointed out, however, that group one (the fastest group of neutrons) is the least important group, the control rods being almost transparent to neutrons in this group and absorption very small compared to the three lower energy groups.

24

TABLE V
Comparison of LEOPROD and NUS values
for MH-1A Control Rods

LEOPROD values:	group	$\langle\alpha\rangle$	$\langle\beta\rangle$
	1	.0009008	361.4
	2	.004122	78.24
	3	.1256	2.215
(Wigner-Wilkins)	4	.4974	.5022
NUS - 576 values	group	$\langle\alpha\rangle$	$\langle\beta\rangle$
	1	.004394	756.23
	2	.004161	77.95
	3	.1259	2.2086
(Wigner-Wilkins)	4	.4979	.5022

The agreement of LEOPROD results with those of NUS (Ref 7) gives one confidence in the methods employed in the calculation of $\langle\alpha\rangle_n$ and $\langle\beta\rangle_n$.

Table VI presents a comparison of values of D and Σ_a calculated by LEOPROD using the discrete mesh formula (with h=t) and using the continuous media formula. It can be observed from Table VI that the values for groups 1 and 2 are not altered by using either the continuous model or the discrete one. This is as expected, since the mesh size is much smaller than the mean free path in the control rod for neutrons in these two groups. Thus, for neutrons in these two groups, any mesh size is equivalently zero and the medium appears continuous. The mesh size does influence the values for the third group, and its effect is greatly enhanced for the fourth, or thermal group. The conclusion drawn from this result is that the continuous media equations are applicable only when $\dfrac{\langle\alpha\rangle_n}{\langle\beta\rangle_n} \ll 1$.

TABLE VI

LEOPROD Results for MH-1A Control Rods

Neutron Energy Group	Continuous Media		Discrete Mesh	
	D(cm)	$\Sigma_a(cm^{-1})$	D(cm)	$\Sigma_a(cm^{-1})$
1	114.7	.002837	114.7	.002837
2	24.84	.01298	28.84	.01298
3	.6896	.4034	.6831	.4015
4 (WW)	.05169	4.837	.01478	2.870
4 (MND)	.09921	9.284	.02837	5.509

One further consideration serves to minimize the group 1 discrepancies between LEOPROD and NUS (Ref 7). Namely, the fundamental quantity in the continuous media formalism is the product of $<\alpha>_n$ and $<\beta>_n$. On this basis, though $<\alpha>_1$ and $<\beta>_1$ individually are different in the LEOPROD and NUS calculations, $<\alpha>_1 \times <\beta>_1$ is nearly the same for both. Physically, this implies that both calculations result in the same quantity for total loss of group 1 neutrons, the difference being only in the relative sizes of the loss through leakage and the loss through absorption. This fact increases confidence in LEOPROD's results.

The values of D as given by blackness theory are predicated on the assumption of negligible scattering. This holds true in a pure absorber. However, in a physically realistic case, such as the MH-1A control rods, the pure absorber is dispersed in a stainless steel matrix. The steel has nonnegligible scattering properties (and makes up ≈ 96 v/o of the control rod) while the boron-10 is essentially a pure absorber. Thus a justifiable approximation is to take the values for D from those for stainless steel for certain cases which satisfy a physical rationale. These cases are discussed in detail in the next section. Three cases are considered:

(a) rods all in.

(b) rods all out.

(c) rods at some intermediate position.

26

Boron-10 is a strong thermal absorber (i.e. its main effect is upon group 4 neutrons). Thus, the D values used for groups 1 and 2 are those corresponding to stainless steel for all three above cases. The D values for group 3 in the rods-in case were taken from blackness theory, while for the other two cases, pure stainless steel values were used. The blackness theory D value was used for group 4 in all three cases except for the outer borated rod followers (in the rods-out case) which were representable by stainless steel D values due to the low boron-10 number density there.

Table VII gives the MH-1A rod constants used, with the pure stainless steel D values obtained from a LEOPARD calculation and the blackness theory D values obtained with LEOPROD. The Σ_a values are all obtained from a LEOPROD calculation and thus based on blackness theory.

TABLE VII

MH-1A Control Rod Constants Used

Group	D(cm)	$\Sigma_a(cm)^{-1}$
1	1.615	.002837
2	.9048	.01298
3	.3609 (.6831)*	.4015
4	.3556 (.01478)*	2.870
4	.6825 (.02236)*	5.509

* Blackness theory values

Care must be exercised in obtaining the MND values for stainless steel. The unit cross-section used to obtain the MND values from the Wigner-Wilkins cross-sections should be characteristic of the fuel cell spectrum (since the entire reactor is represented by this equivalent LEOPARD fuel cell) and not of a pure stainless steel cell spectrum.

In order to perform the calculation for rods-out k_{eff}, one must obtain the equivalent diffusion theory constants for the borated followers. The results of a LEOPROD calculation for the inner followers (0.16 w/o natural boron) are presented in Table VIII, and for the outer followers (0.06 w/o natural boron in Table IX. The

27

number densities used in these calculations are presented in Table X, where the follower boron-10 number densities are the equivalent boron-10 values obtained as explained in Section IV B, and the stainless steel values are for pure SS-348. The D values used for the followers are those given in Table VI for stainless steel with the exception of the thermal group value (1.902 cm) used for the inner followers which was obtained from LEOPROD.

In summation, the LEOPROD program calculates the equivalent diffusion theory constants for control rods. There is good confidence in the numbers calculated for Σ_a and, together with the proper choice of stainless steel values for the diffusion coefficient when valid, the results of LEOPROD may be used to represent control rods in few group diffusion theory programs such as TURBO*.

TABLE VIII

MH-1A Inner Rod Follower Constants

group	$<\alpha>$	$<\beta>$	$\Sigma\, a(cm)^{-1}$
1	$.6545 \times 10^{-4}$	$.4945 \times 10^{4}$	$.2062 \times 10^{-3}$
2	$.6686 \times 10^{-4}$	$.4846 \times 10^{4}$	$.2106 \times 10^{-3}$
3	$.6682 \times 10^{-2}$	47.40	.02105
4-WW	08737	4.004	.2767
4-MND	.1677	7.685	.5311

TABLE IX

MH-1A Outer Rod Follower Constants

group	$<\alpha>$	$<\beta>$	$\Sigma\, a(cm)^{-1}$
1	15690×10^{-4}	$.5681 \times 10^{4}$	$.1793 \times 10^{-3}$
2	$.2520 \times 10^{-4}$	$.272 \times 10^{5}$	$.7936 \times 10^{-4}$
3	$.4358 \times 10^{-2}$	73.42	01373
4-WW	.05780	6.317	.1825
4-MND	.1109	12.12	.3493

28

TABLE X

Control Rod and Rod Follower Number Densities

Element	Inner Follower	Outer Follower	Rod
Boron 10	$.996 \times 10^{-4}$ $(.279 \times 10^{-4})*$	$.374 \times 10^{-4}$ $(.899 \times 10^{-5})*$	624×10^{-2}
Iron	.05854	.05854	.0480
Nickel	$.9950 \times 10^{-2}$	$.9950 \times 10^{-2}$	$.782 \times 10^{-2}$
Chromium	.01606	.01606	.013210
Manganese	$.1736 \times 10^{-2}$	$.1736 \times 10^{-2}$	$.143 \times 10^{-2}$

* Indicates depleted follower
(all in units of 10^{24}/cm)

29

V. METHODS OF ANALYSIS AND RESULTS

A. Introduction

TURBO* (Ref 8), a two-dimensional, few group diffusion theory depletion code, was the basic calculational tool employed. The code allows a performance to the depletion calculation in x-y geometry.

The reactor model to be studied is represented in x-y geometry shown in Figure II-2. The geometry is further defined by placing mesh lines parallel to the two coordinate axes. This divides the reactor into a number of mesh rectangles. The intersection of mesh lines define mesh points. TURBO* can employ up to 7500 mesh points.

The rectangles are grouped into a smaller number of compositions, applying the term composition to all those which, initially, can be described by the same isotopic number densities, self-shielding factors, and buckling. The input to the code consists of the geometric description, self-shielding factors, four group cross-sections, U-238 resonance escape probabilities and nuclide number densities in each composition. This information is used to compute the four-group constants for each composition. Then, the four-group diffusion theory solution for the neutron flux distribution is calculated to determine the beginning of life flux and power shapes. The flux shape is used to compute depletion of each of the burnable isotopes at each mesh point over a specified period of time. The magnitude and spatial distribution of the neutron flux are assumed to be invariant over this time step.

In the MH-1A analysis, a half core calculation was done with 7320 mesh points (120x61), and 30 regions. These regions were made up by seven control rod regions, sixteen consisted of fuel elements, and seven containing various proportions of steel and water. To calculate the number densities in these homogenized regions of steel and water, LEOPARD number densities were used: 100 percent H_2O being 2.67×10^{-2}; 100 percent stainless steel consisting of Fe (5.854×10^{-2}), Ni (9.550×10^{-3}); and the mixed SS-H_2O regions were obtained by multiplying the volume fraction times the appropriate 100 percent number densities. The shuffled core number densities for the fuel elements were obtained as the final values of the TURBO* depletion runs for the original core. The other starting number densities were obtained from LEOPARD. After the first time step, the number densities used at any subsequent time steps are precisely the ones that TURBO* calculates and preserves on the history tape.

30

TABLE XI

SS-H₂O Compositions

Composition Number Used in TURBO*	Description	SS vol fraction	H₂O vol fraction
13	reflector	.50	.50
14	water gap	0.0	1.0
15	rod clad	.2475	.7525
16	inner rod tip	.1222	.8778
17	outer rod tip	.1470	.8530
18	SS filler and H_2O	.5217	.4783
19	SS filler and H_2O	.4720	.5280

The control rods were presented by both a depletable and a nondepletable nuclide. The depletable nuclide was B-10 which was represented as element 29 in the TURBO* program. The nondepletable nuclide was a fictitious element for which the cross-sections used were the macroscopic ones for stainless steel with a number density of unity.

B. Core 2, BOL Calculations

The BOL calculations for core 2 are presented in this section. These calculations were done for: (a) The control rods all the way in, (b) the control rods all the way out.

A brief discussion was presented in an earlier section on the control rods constants and tables of values used for the different cases. Some additional analysis was required to choose D values for the control rods.

Now, $D = 1/3 \, (\Sigma_{tr})^{-1}$ which for the rods is

$$D = 1/3 \, [N_1 \sigma_{tr_1} + N_2 \sigma_{tr_2}]^{-1}$$

where the subscript 1 refers to the nondepletable nuclide (stainless steel) and the subscript 2 refers to the depletable nuclide (Boron-10). The desired approximation is that:

$$D = 1/3 \, [N_1 \sigma_{tr_1} \, (1 + \frac{N_2 \, \sigma_{tr_2}}{N_1 \, \sigma_{tr_1}}) \,]^{-1}$$

$$\simeq 1/3 \, [N_1 \sigma_{tr_1}]^{-1}$$

which requires that $\dfrac{N_2 \sigma_{tr_2}}{N_1 \sigma_{tr_1}} << 1.$

31

In the present analysis, $N_1 = .0639$ and the value of N_2 depends on the position of rods in the core. The values of $N_2 = .624 \times 10^{-2}$ (rods-in core); $N_2 = .996 \times 10^{-4}$ (rods out, outer followers) and $N_2 = .374 \times 10^{-4}$ (rods out, inner followers). The appropriate σ_{tr} values of a LEOPARD calculation with isolated B-10 and SS-348 (i.e., self shielding effects neglected) are presented in Table XII.

TABLE XII

Microscopic Transport Cross-Sections, Barns

	Group 1	Group 2	Group 3	Group 4
B-10	2.46	5.97	38.4	1588
SS-348	2.35	3.85	9.62	11.3

An engineering judgment is utilized such that when the above ratio is greater than 0.20, only blackness theory values can be used. In other situations, i.e. the ratio less than 0.20, the stainless steel approximation can be used. On this basis, it is found that the outer followers can be represented by a stainless steel approximation for all the four groups, and the inner followers for the three fast groups. In the rods-in case, the stainless steel approximation is valid only for the two highest energy groups. The values of the ratio $\dfrac{N_2 \sigma tr_2}{N_1 \sigma tr_1}$ are presented in Table XIII.

TABLE XIII

Ratio Criterion

	Group 1	Group 2	Group 3	Group 4
Rods out inner	1.64×10^{-3}	2.42×10^{-3}	6.22×10^{-3}	.220
Rods out outer	$.614 \times 10^{-3}$	$.907 \times 10^{-3}$	2.33×10^{-3}	.0825
Rods in	0.103	0.151	.390	14.1

Table XIV presents the calculated k_{eff} and compares it with those obtained for Core 1. These calculations were done with MND cross-sections.

32

One notices an increase in the value of k_{eff} (rods-out) between Core 1 and Core 2. The reason for this difference lies in the fact that the inner elements of Core 2 (the outward elements of Core 1 shuffled inward) have an average enrichment of 4.22 percent compared to 4.07 percent of Core 1. In addition, the Core 2 calculation used analytically derived blackness theory control rod constants which were significantly larger than the NUS suggested values used in Core 1 calculations. Thus, the increase in k_{eff} due to increased enrichment is somewhat obscured by the larger control rod absorption constants. In fact, the latter is reflected in the k_{eff} values of Core 2 for the rods-in case which is smaller.

TABLE XIV

Comparison of k_{eff} Values Between Core 1 and Core 2.

BOL, k_{eff} (490°F)			
	Core 1 New C Rods	Core 2 New C Rods	Core 2 New C Rods & Poison Shims
Rods in	.873	.871	.8663
Rods out	1.055	1.057	1.043

The rationale behind the choice for the ratio criterion to be 0.20 is clearly verified by the k_{eff} values obtained for the rods-in and rods-out cases using the stainless steel modification value for D in all the groups. This effect of D on k_{eff} is presented in Table XV. It is noticed from this table that when the ratio is much greater than 0.20 the all-stainless steel D calculation gives an appreciably different answer than the one using blackness theory.

Table XIV presents two values for Core 2, one of which is with the use of new control rods and poison shim pins. Core 2 contains the poison shim pins. The depletion study, discussed in the next section analysis includes the representation of the core with the poison shim pins.

33

TABLE XV

Effect of D values on k_{eff}

	All SS D	Mixed D	Ratio criterion for group 4
Rods In	.865	.871	24.1
Rods Out	1.059	1.057	.22

C. Core Depletion (Preliminary Studies)

The analysis of a nuclear reactor requires determination of the reactor's characteristics throughout its operating history. These characteristics include the distribution of power throughout the core, the concentration of various nuclides at different locations in the reactor, and the control rods position required for criticality, plus many others. The examination of depletion effects is a complex task requiring use of many approximations and giving rise to a large number of alternative approaches. Common to all of these approaches, however, is a depletion cycle. This cycle consists of calculations of microscopic cross-sections, spatial flux and power distributions, flux and power editing, depleted number densities.

Core 2 depletion was performed in the following manner. An artificial rod bank position was chosen at the first time step so that the starting k_{eff} was 1.014. At each time step, the k_{eff} calculation was performed twice; once with the initial number densities, and next with the final number densities for that time step. The difference in these two k_{eff} values was the Δk_{eff} associated with that time step. The successive Δk_{eff} values were subtracted from the BOL rod out k_{eff} value, to yield k_{excess} as a function of time. On this basis, the end of core life was defined to be that time when

$$\sum_i (\Delta k_{eff})_i = k_{excess} \text{ at BOL; } i = \text{time step number}$$

The artificial rod bank position formalism was introduced in an attempt to represent the physical three-dimensional reality in a two-dimensional calculation. The rationale was to duplicate a change in rod bank position by a change in number densities in the control rod compositions. For the rods-in case (fractional withdrawal = 0.0), the control rod number densities of Table X are used (let this be N_I). If N_o is defined as the pure stainless steel number densities, then for compositions consisting of stainless steel and control rod we have:

34

$$N = N_I + X (N_o - N_I)$$

with X defined as the fractional withdrawal of the rod bank.
The boron-10 number density is: $N_b = 6.24 \times 10^{-3} (1-X)$. These equations
provided the number densities for input into the LEOPROD calculations
which yielded the graphs of Figures V-1 through V-3. The values in
Figures V-1 through V-3 for X=1.0 (i.e. rods-out) do not represent
precisely the LEOPROD calculation. Instead they are average values
of the LEOPROD results calculated separately for inner and outer
followers (due to different boron number densities). In the rods-out
TURBO* calculation the precise Σa values were used, not this average
one.

Strictly speaking, the rod bank "position" (i.e. x) defined in this
manner is an artificial quantity. In reality, for the rod bank at x,
(1-x) times the core height in the rod regions consist of the large
boron number density control rods, while the remainder is all borated
followers. In the two-dimensional equivalent, the entire core height
in the rod regions consists of the average number densities calculated
by the above two equations. Obviously, in terms of reactivity effect,
the two cases are not identical (i.e., rod bank withdrawal of X does
not result in the same k_{eff} if the problem were truly solved in the
full three dimensions). However, this artificial scheme has the
virtue of coupling the four group Σ_a values. That is, in hunting
for the appropriate Σ_a for a desired k_{eff}, one must choose four Σ_a
values, one for each group, in a rational manner. It would be un-
justified to choose Σ_{a1} corresponding to X = .60, Σ_{a2} corresponding
to X = .78, etc., in a single calculation. Thus the artificial rod
bank position formalism provides a method whereby consistent four
group Σ_a values may be chosen, even though this artificial bank posi-
tion does not, in itself, have a strict physical analogue (except for
the rods-in and the rods-out cases).

The desired k_{eff} for the start of the first time step was obtained
with X at 0.91. Carrying out the same type of analysis of $\frac{N_2 \sigma tr2}{N_1 \sigma tr1}$ as
in Part B, one finds that the 0.20 criterion is exceeded only for
group 4. As the core depletes, X increases beyond 0.91 and $\frac{N_2}{N_1}$ decreases,
thus the 0.20 criterion can never be exceeded in the fast group. In
the thermal group, the ratio starts at 2.62 and decreases over the
depletion, but always remains greater than 0.20 since σ_{tr2} is so large
compared to σ_{tr1}. Thus stainless steel D values are used for the fast
groups, and blackness theory D value for the thermal group, throughout
the depletion analysis.

Figure V-4 indicates the particular k_{eff} calculated at the beginning
and at the end of the time step. At the end of the third time step
(50 full power days), the k_{eff} had fallen to 0.986; thus a readjustment
of the boron-10 number density was required to bring k_{eff} close to 1.0.

FIGURE V-1   BLACKNESS THEORY Σ_a VALUES
VS. ARTIFICIAL ROD BANK POSITIONS

FIG V-1a Σ_a FOR GROUP ONE

FIG V-1b Σ_a FOR GROUP TWO
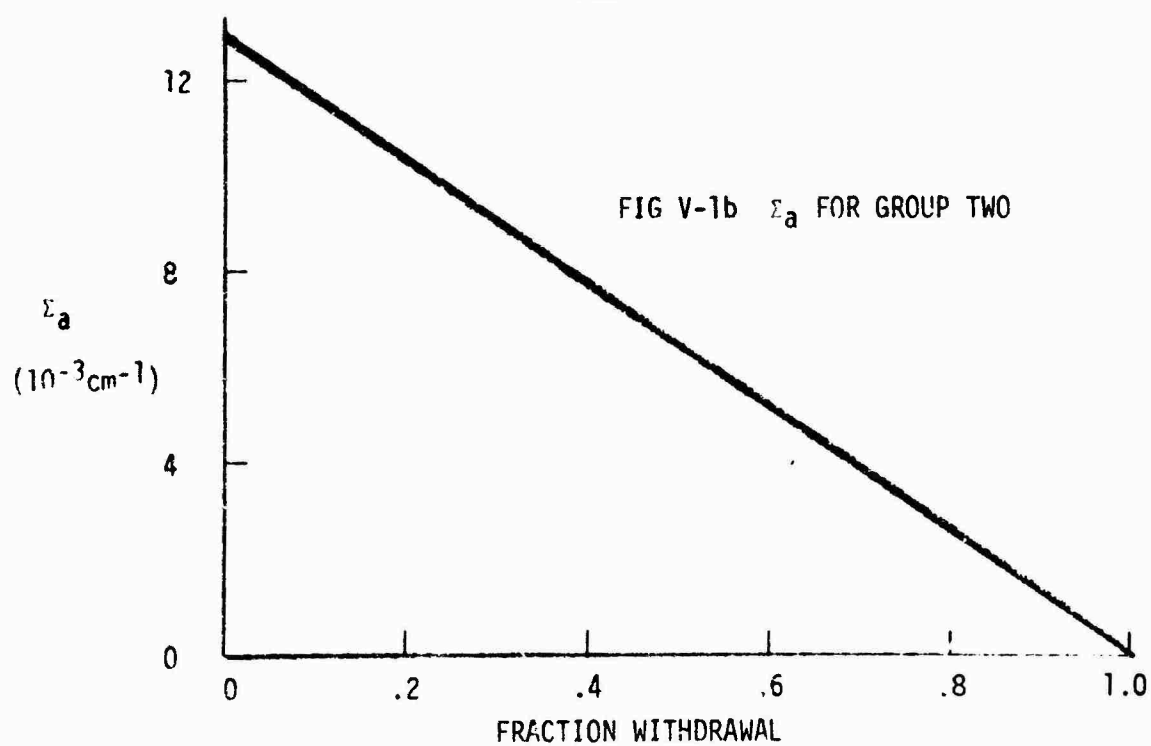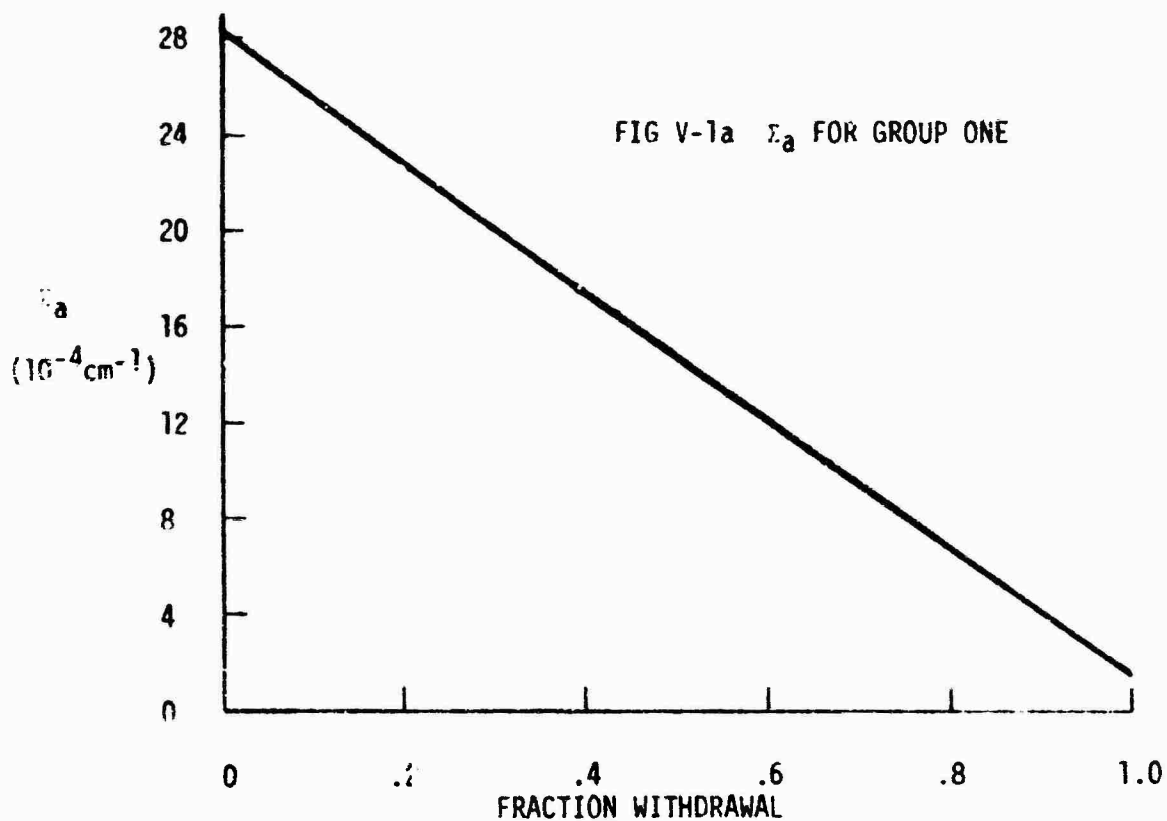
FIGURE V-2. BLACKNESS THEORY Σ_a VALUES
VS. ARTIFICIAL ROD BANK POSITIONS

FIG. V-2a Σ_a FOR GROUP THREE

FIG. V-2b Σ_a FOR GROUP FOUR
(WIGNER-WILKINS)
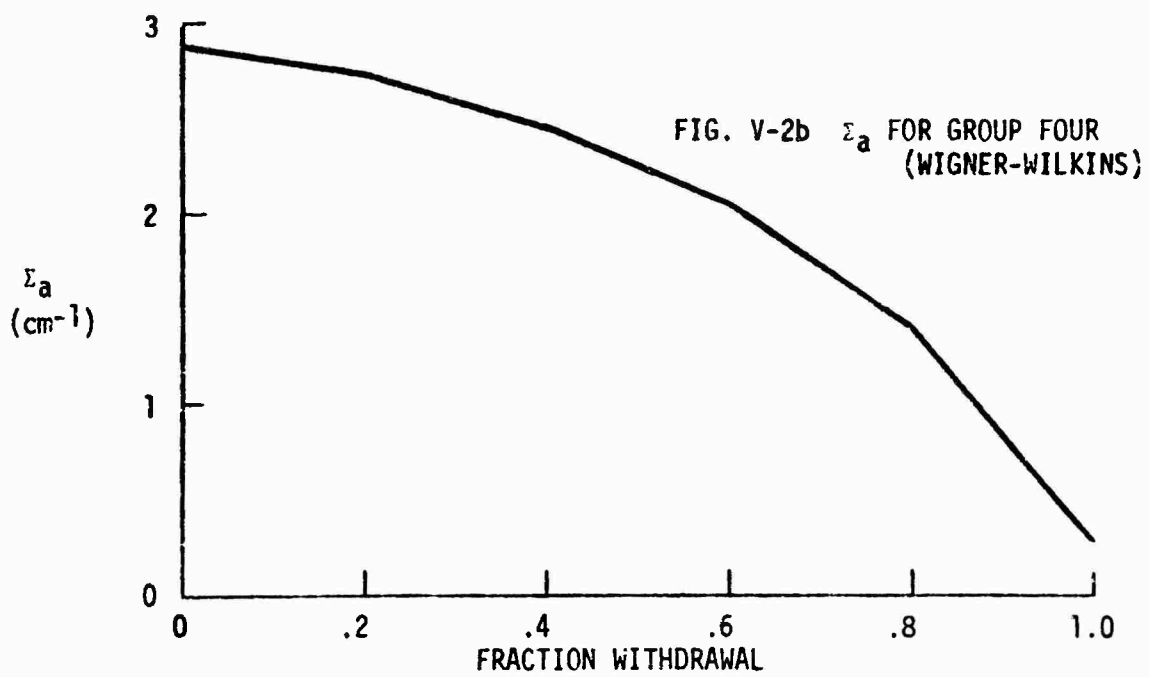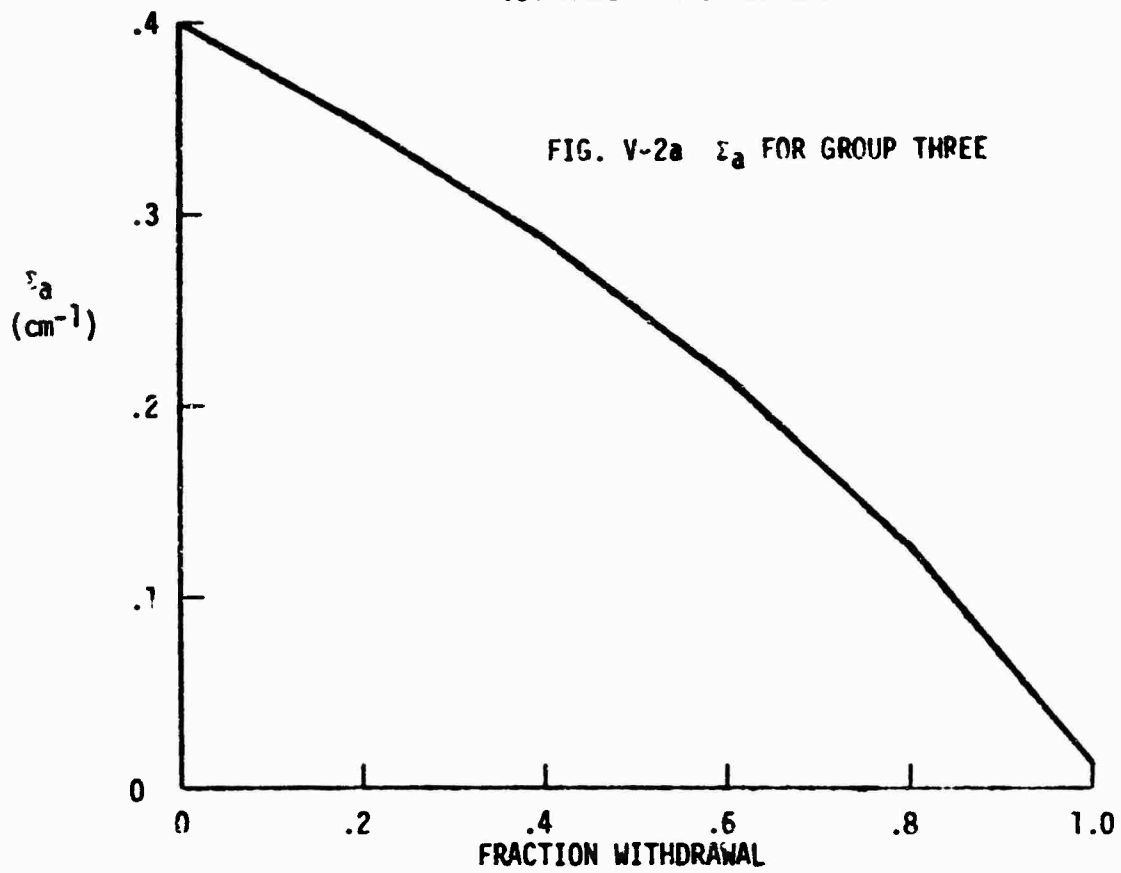
FIGURE V-3 BLACKNESS THEORY Σ_{+r} VALUES VS. ARTIFICIAL ROD BANK POSITIONS

FIG. V-3a Σ_{+r} FOR GROUP 3

FIG. V-3b Σ_{+r} FOR GROUP 4 (WIGNER-WILKINS)

38

FIG. V-4 k_{eff} VS. TIME STEPS
HALF CORE TURBO

FULL POWER DAYS

39
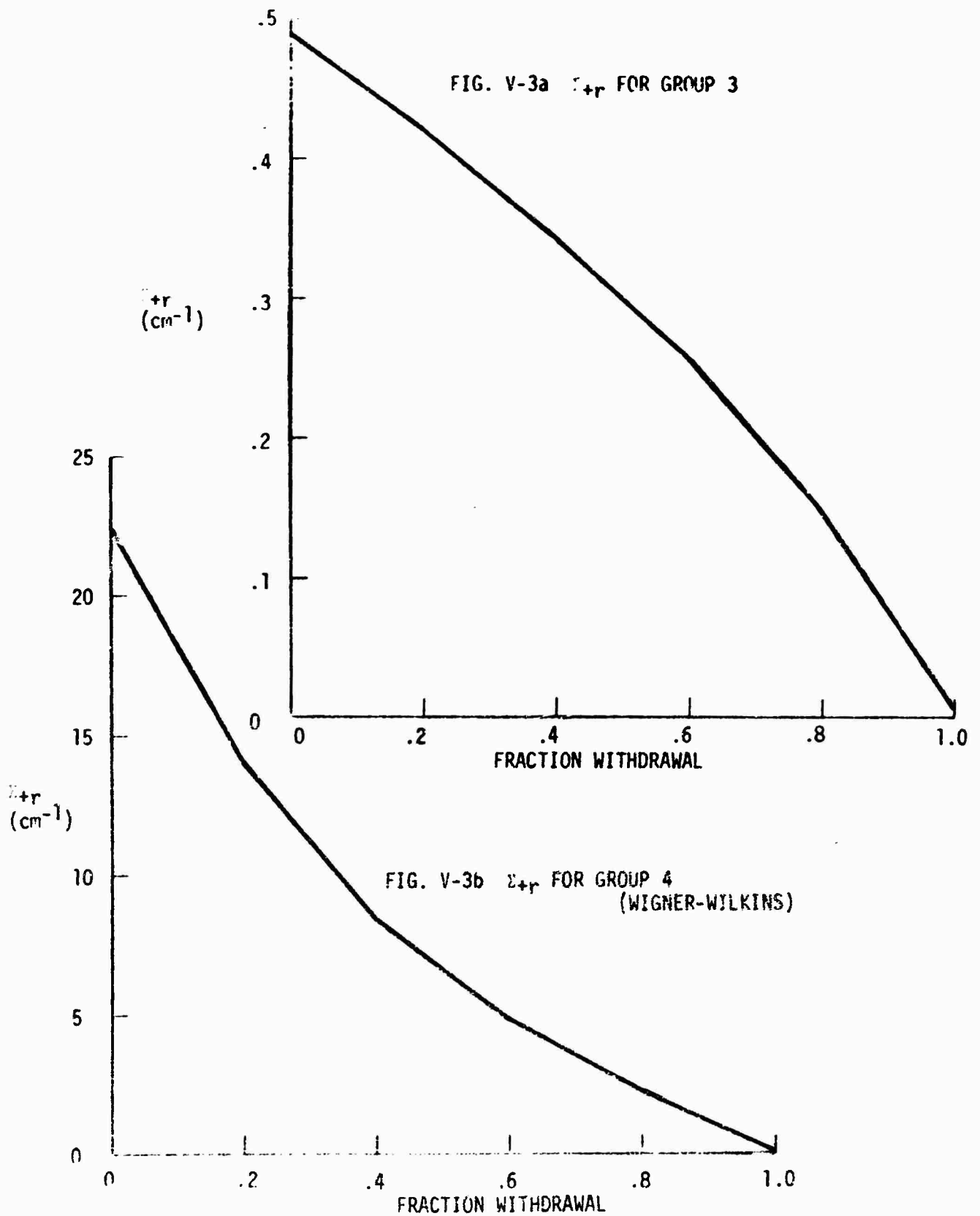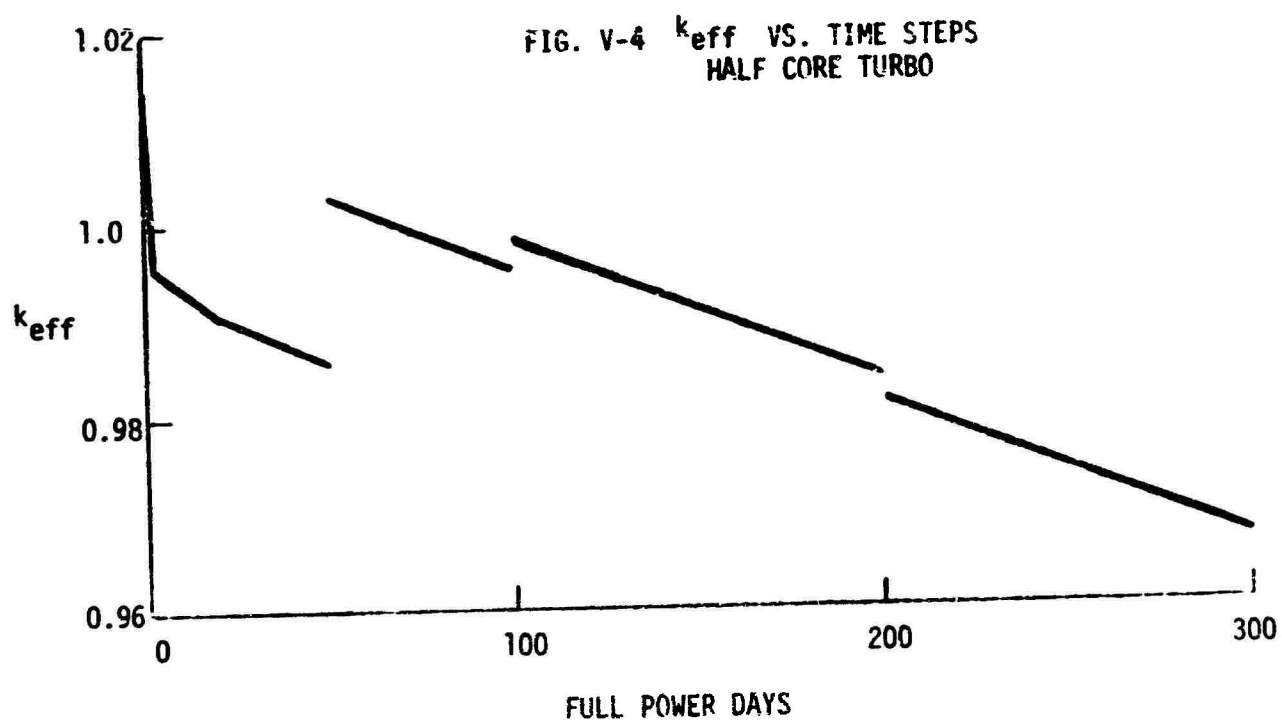
Simulating a rod bank withdrawal, the number density was reduced to 8.0×10^{-2} which yielded a k_{eff} of 1.0027. Again the depletion was continued further, with composition-wise homogenization of the number densities. The discontinuities present in Figure V-4 beyond 50 full power days are due to the change in the cross-sections with each time step.

Figure V-5 indicates the behavior of k_{excess} (rods-out k_{eff}) as the depletion proceeds. The k_{excess} values are obtained by subtracting the k_{eff} for each time step (given in Figure V-4) successively, as described earlier.

D. Quarter Core Depletion Study (Core 2)

The preliminary calculations discussed previously have not accounted for the existence of the 12 poison shim pins located at the meeting of the control rod tips. These poison shim pins were originally loaded in the shuffled core on the assumption that the original control rods (which had experienced marked depletion in the follower regions) would be reused. However, during reloading, cracks were discovered in the control rod blades; thus, an entire new set of control rods were installed. The 12 poison shim pins remained in the core after the replacement of the control rods. The poison shim pins extended for the full height of the core.

This depletion was done with a quarter core configuration to minimize the usage of computer time. The 12 poison shim pins were explicitly represented in the quarter-core analysis. Due to the shuffling scheme, the core is not strictly quarter-core symmetric. Some idea of the discrepancy in k_{eff} between a quarter-core and half-core solutions may be obtained by comparing identical situations. For these situations, the half-core BOL k_{excess} calculated was 1.0518; the quarter core value was 1.0484. This difference is due primarily to the distortion of the flux shape along the new boundary created by the quarter-core representation. This representation has a built-in uncertainity in defining end of core life which will be discussed.

The reactivity worth of the poison shim pins was evaluated by doing two TURBO* calculations. One with 1 weight percent of B-10 present in the shim pins and the other with B-10 replaced by stainless steel. The values between these two cores is equivalent to the worth of the shim pins. This is found to be equal to .947 percent $\Delta k/k$ at BOL.

The next few paragraphs present a brief discussion on the manner of manipulating the poison shim pins in the calculations as well as the choice of control rod constants.

Element 17 (not fixed on the history tape) was used as a variable poison in the control rod regions. Its number density was manipulated to keep k_{eff} in the desired range throughout the depletion. Its cross-

FIG. V-5 k_{EXCESS} VS. BURN-UP
HALF CORE TURBO
DUMMY SS SHIM RODS

41
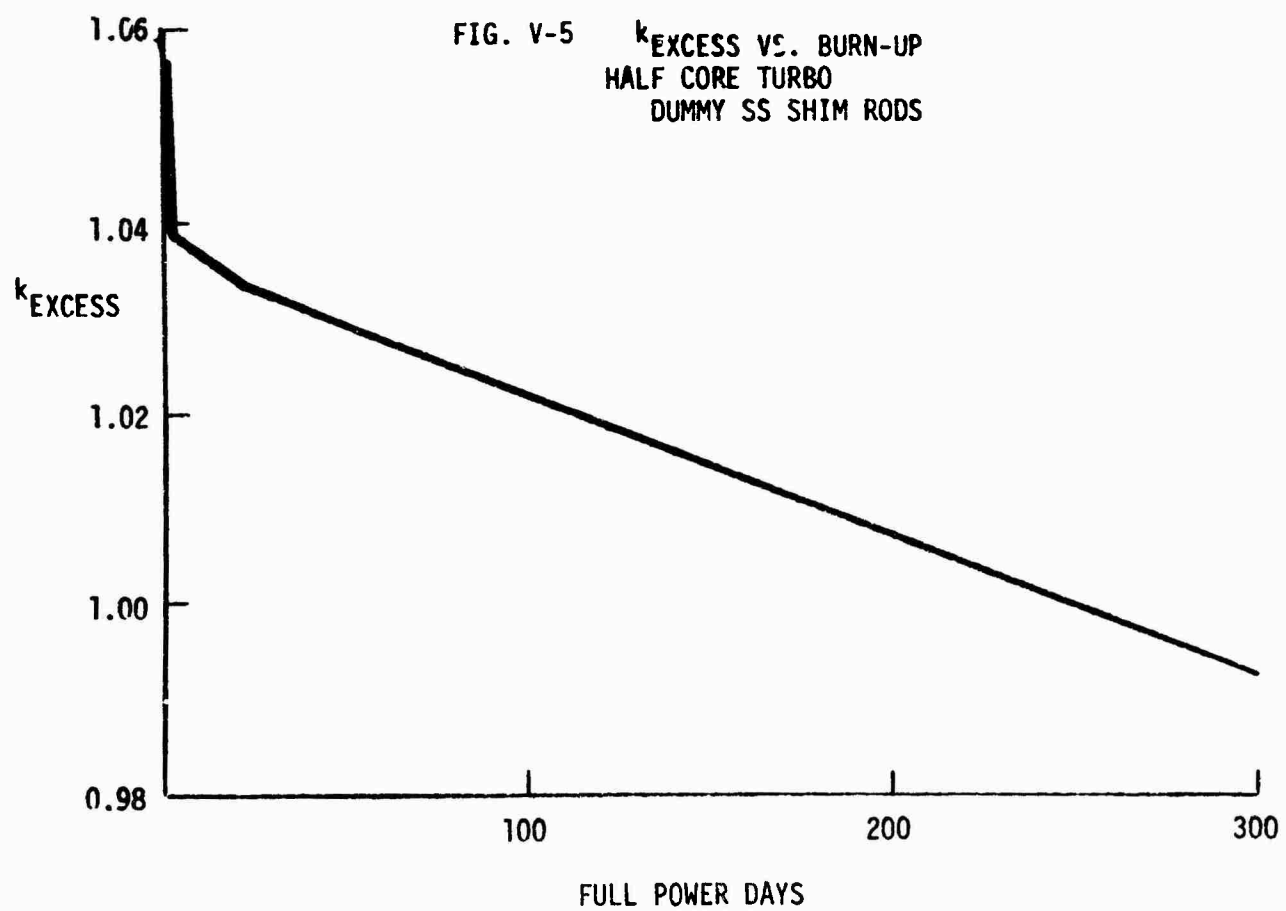
sections are identical to those used for the control rods in the half-core depletion analysis. Element 29 was used for the depletable boron in the inner followers and the shim rods (1 w/o B), while element 30 was used for the depletable boron in the outer followers. All cross-sections were the blackness theory and pure stainless steel values chosen as in the half-core analysis. Unlike the half-core depletion analysis, the boron number densities in the followers are kept distinct from those in the control rod sections; thus, the depletion of the follower and shim rods is represented explicitly.

Element 12 was used to input the stainless steel constants in the control rods, followers, and shim rods. Thus if the blackness theory constant in a follower region is Σ_{ai}^{BT} and the stainless constant is Σ_{ai}^{SS}, then the boron-10 constant in that region for group 1 is defined:

$$\sigma_{ai}^{B} = \frac{1}{N^{B}} \; (\Sigma_{ai}^{BT} - \Sigma_{ai}^{SS})$$

where N^{B} is the BOL boron-10 number density in the region. When all the boron-10 has been depleted in the region, the region is characterized by pure stainless steel constants. Note that this formalism tends to underestimate the boron-10 depletion since σ_{ai}^{B} is calculated from BOL conditions; thus BOL self-shielding factors for boron-10 are used throughout the core-life. In reality, the degree of self-shielding reduces as the boron-10 is depleted thus, σ_{ai}^{B} at later time steps is larger than the value calculated above, and the boron-10 depletes more rapidly than calculated. This implies that the calculated core life is a lower bound on the true core life. In any event, this difference is decidedly a minor point.

In order to obtain the blackness theory constants for the shim rods, the cylindrical geometry must be properly represented in LEOPROD. The fundamental geometrical quantity in considering absorption is the mean chord length: $\overline{L} = 4V/S$, where V is the volume of the lumped absorber and S is its surface area (see pg. 715 ff of Reference 9). LEOPROD handles slab geometry absorbers (the geometrical input being the slab thickness). For a slab we have: $\overline{L} = \dfrac{4ab\ell}{2(a\ell+b\ell+ab)} = \dfrac{2a}{1+a/b+a/\ell}$ where a is the slab thickness, b the slab width, and ℓ the slab length. The LEOPROD calculation assumes an infinite slab for which:

$$L^{\infty} = \lim_{\substack{b\to\infty \\ \ell\to\infty}} \left(\frac{2a}{1 + a/b + a/\ell}\right) = 2a.$$

Thus, the geometrical input into LEOPROD is one-half the mean chord length.

For a cylinder, $\overline{L} = 2r$, r being the radius. Thus to obtain the appropriate blackness theory constants for the shim rods, the required geometrical input quantity is the shim rod radius. For the MH-1A case,

42

this result is convenient since the shim rod radius is approximately equal to control rod absorber thickness, and the same geometrical input may be used in LEOPROD for both regions.

The technique of predicting core life was quite similar to the discussions presented in the previous section. Figure V-6, a graph between k_{excess} versus burnup, was used to predict core life. A short discussion on uncertainties on such predictions and the differences in core life for the first two MH-1A cores is presented in the succeeding paragraphs.

To return to the discussion of uncertainities in the TURBO* calculation: Recall that the difference between half-core and quarter-core calculations of BOL k_{excess} calculation is the worst possible assumption since it would be more likely that the difference would decrease with burn-up; the depletion process is one which seeks a natural asymptotic equilibrium (i.e. larger flux at a point depletes the fissionable elements there more quickly, which in turn reduces the flux). On this assumption, the maximum deviation from the calculated end of core life datum is 24 days. Thus the core life is predicted to be 253±12 full power days. This is to be compared with the half core, dummy shim rods, value of 250 full power days. The implication is that the shim rods have little effect on the overall core lifetime, their primary purpose being to provide reactivity holddown at BOL.

After all the data of Figure V-6 had been obtained and the EOL point of 241 days established, the sixth time step was repeated, only this time from 200 to 241 full power days (rather than 200-300 full power days). Taking the final number densities at the end of 241 days, the calculation of k_{eff} with all rods out was made, yielding a value of 1.00070. The good agreement of this value with the expected one of exactly 1.0 at EOL demonstrates confidence in the technique of k_{eff} summation for each successive time step. This deviation of EOL k_{excess} implies an error of three full power days (i.e. assuming a linear behavior of k_{excess} if k_{excess} = 1.00070 at 241 full power days, it will be 1.0 at 244 full power days). Thus the uncertainty in defining EOL due to the k_{eff} technique (± 3 days) is well with the maximum estimated uncertainty (± 12 days) due to asymmetry considerations.

The explicit representation of the boron-10 in the followers allows TURBO* to calculate the boron depletion in the rod followers. Over the core life, the quarter-core calculation indicated that two inner followers depleted to 49.07 percent and 54.06 percent of the initial boron number densities; that the two outer followers depleted to 53.05 percent and 54.38 percent of their initial number densities.

Table XVII presents the average enrichments (w/o u-235) for the two different enrichment regions for the three cores. From the fact that the average enrichment of the inner region (the shuffled elements retained from the previous core) varies from core to core, one may

43

MH-1A CORE 2 DEPLETION

FIG V-6 k_{EXCESS} VS. BURN-UP
WITH 1% B SHIM RODS

FULL POWER DAYS

44
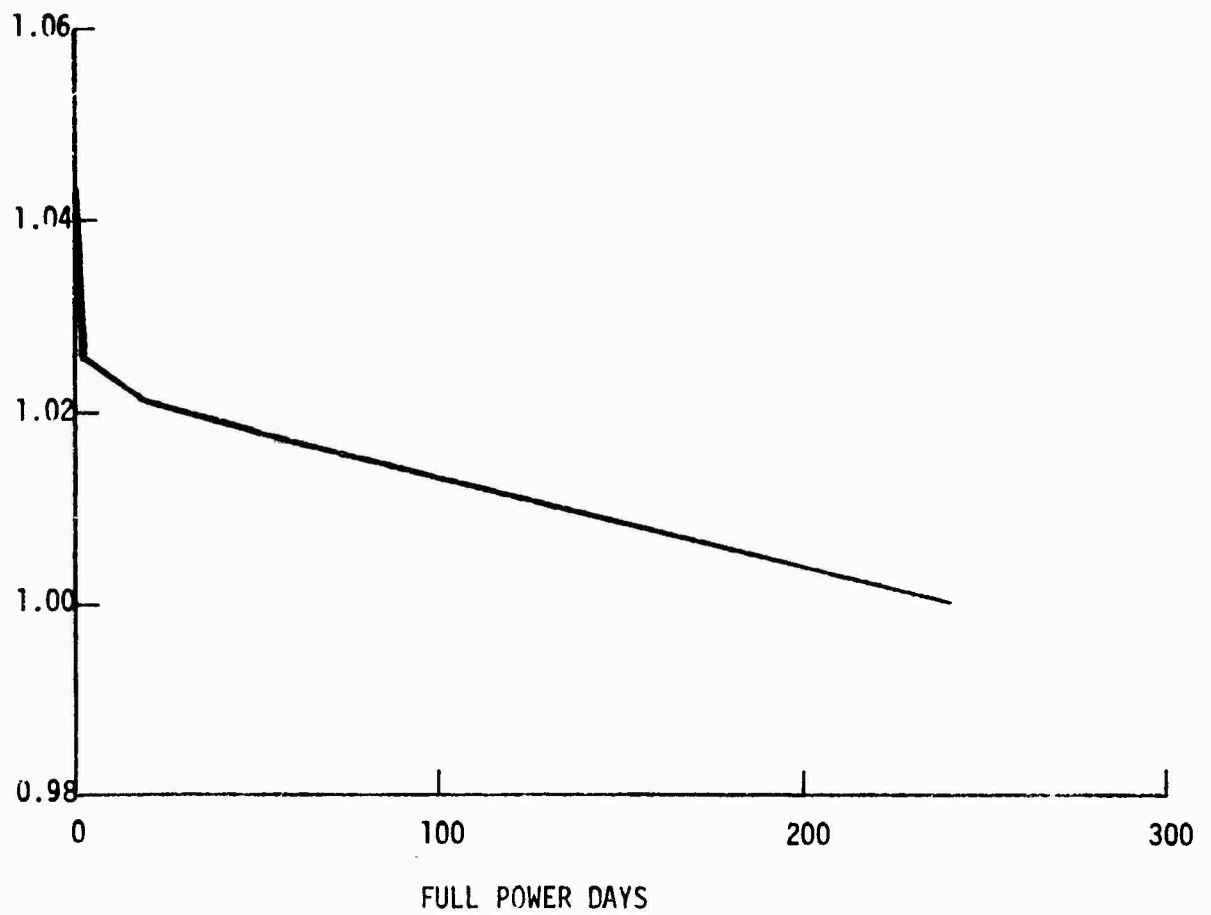
conclude that an equilibrium core design has not been achieved. This in turn causes the marked difference in the core life for the first two cores. Also it may be remarked that Core 2 experienced a significant decrease in inner region burn-up. For Core 1, the outer design depleted by 0.432 percent and the inner by 0.756 percent; while for Core 2, the outer region depleted by 0.305 percent and the inner by 0.474 percent. Note the degree to which the Core 2 integrated flux is "flatter" (i.e. the amount of fuel depleted in the two regions is more nearly the same). This effect is attributed to the poison shim rods and fission product poisons present at BOL in the inner region of Core 2, both tending to decrease flux peaking in the inner region.

TABLE XVI

Control Rod Number Densities

Burn-up	B-10 Number density	B-10 Number density
(Full power days)	Inner rod	outer rod
0	$.119 \times 10^{-2}$	$.119 \times 10^{-2}$
50-	$.1159 \times 10^{-2}$	$.1169 \times 10^{-2}$
50+	$.80 \times 10^{-3}$	$.80 \times 10^{-3}$
300	$.7336 \times 10^{-3}$	$.7548 \times 10^{-3}$

TABLE XVII

Comparison of Region-wise Average Enrichment

	Inner Region	Outer Region
BOL Core 1	4.07%	4.65%
EOL Core 1	3.314%	4.218%
BOL Core 2	4.218%	4.65%
EOL Core 2	3.744%	4.345%
BOL Core 3	4.345%	4.65%

TABLE XVIII

Some Properties of Core 2

Core Life = 253±12 full power days

Worth of 12 poison shim rods (1%B) @ BOL = 0.947% k/k

E. Core 3, BOL Calculations

The final number densities as given by TURBO* at the conclusion of the 20 day xenon decay calculation at trend of core life for Core 2 provide the starting point for the Core 3 calculations. The TRBOR routine of TURBO* was used to shuffle and rotate the outer fuel elements inward and also to insert fresh fuel elements in the outer positions. The quarter-core configuration permitted the shuffle, rotation, and refueling to be "performed" in a single TRBOR run. The result was a new core model which duplicated that obtained by physically reloading Core 2 as per the refueling scheme (Appendix A of Ref 10).

The cross-sections for the new core were obtained through a LEOPARD calculation which used the TURBO* number densities for Core 3 at BOL. Again, the control rod constants were obtained by LEOPROD: The absorber cross-sections were the same as those used for Core 2 (i.e., the control rod absorber sections were assumed to be essentially undepleted), while the borated followers were assigned new cross-sections to reflect the decreases in the boron-10 self-shielding effect due to depletion. Table XIX presents the absorption cross-sections for the boron-10 in the reused rod followers as given by LEOPROD.

TABLE XIX

B-10 σ_a (in barns) for Depleted Followers

Group	Inner followers	Outer followers
1	1.175	2.329
2	2.113	2.123
3	69.82	0.0
4 MND	388.8	877.0

As discussed previously, these values are corrected so that after all the boron-10 has been depleted, the rod follower absorption is that of stainless steel alone.

For the new poison shim rods, the boron-10 number density obtained from lab analysis was input. However, since only two elements in TURBO* are available for use as boron-10 (elements 29 and 30), the boron-10 outer follower cross-sections were used for the shim rods with the difference in self-shielding effects in the two compositions corrected by assigning a self-shielding factor of 0.7052 to the shim rods. Thus the same set of cross-sections yielded the correct macroscopic cross-sections for two different compositions.

As in the Core 2 calculations, the BOL k_{eff} calculations for Core 3 were performed in a quarter-core configuration. Table XX presents the results for Core 3.

TABLE XX

BOL k_{eff} Values - Core 3

	Hot (490°F)	Cold (100°F)
Rods In (Reused Rods)	0.8843	0.9524
Rods Out (Reused Rods)	1.0584	1.1227
Rods Out (Mod. Rods)	1.0911	1.155

The shut-down margins were obtained from TURBO* calculations in which all control rod constants were characterized by the full control rod constants given by LEOPROD to simulate the all-rods-in case. Table XX, shows that the hot (490°F) and cold (100°F) shutdown margins are, respectively, -13.08 percent $\Delta k/k$ and -5.00 percent $\Delta k/k$.

Similarly, from the rods-out valves of Table XX, the excess reactivity at BOL in re-using the previous set of control rods is 5.52 percent $\Delta k/k$ and 10.95 percent $\Delta k/k$ for the hot and cold cases respectively. For the case where Type I modified control rods are installed, the appropriate hot and cold excess reactivities are, respectively, 8.35 percent $\Delta k/k$ and 13.42 percent $\Delta k/k$.

47

In order to obtain the flux shape corresponding to $k_{eff} \sim 1.0$ at BOL in the "hot" state, a critical search was performed. This was carried out by varying the number density of element 17 (given the boron-10 control rod cross-sections) and noting the k_{eff} values calculated by TURBO*. Table XXI presents the result of this progress.

TABLE XXI

Critical Search Results

Number density element 17	k_{eff}
1.0×10^{-3}	1.00858
1.2×10^{-3}	1.00155
1.5×10^{-3}	0.99212

F. Stuck Rod Calculations (Core 3)

The stuck rod calculations were performed by using TURBO* in a full core configuration in which the stuck rod composition was described by stainless steel parameters and the other control rod regions by the rods-in parameters. Table XXII presents the results at the "cold" temperature (100°F).

TABLE XXII

Stuck Rod k_{eff} Values

Outer stuck rod	Inner stuck rod
0.9841	0.9879

It is clear that the stuck rod margin of -1 percent Δ k/k is met. It should be noted that the values of Table XXII are for the reused control rods (in which some boron-10 is present in the depleted followers) and with new poison shim rods present in the core. Without

48

the reactivity hold-down contributed by these two sources, the 1 percent $\Delta k/k$ shutdown margin could not be met. In addition, if Core 2 undergoes less than the 253 full power days of burn-up assumed, the enrichment of Core 3 will be greater than that used in the TURBO* calculation, thus reducing the shutdown margin.

An inner stuck rod calculation was also performed for the case where modified type rods were used (i.e. a stainless steel follower replaces the depleted follower). The resulting k_{eff} was 1.0022 which clearly fails to meet the required shutdown margin.

An uncertainty of 0.1 percent $\Delta k/k$ may be assigned to the above numbers, i.e. a maximum uncertainty of 10 percent in calculating a stuck rod shutdown margin of precisely -1 percent $\Delta k/k$. Industry employs a shutdown margin of -0.3 percent $\Delta k/k$ (considerably looser than the -1 percent $\Delta k/k$ required here), thus an uncertainty of 0.1 percent $\Delta k/k$ (a 1/3 uncertainty) seems adequate to cover inherent uncertainties in the diffusion theory code calculation. Thus the stuck rod shutdown margins calculated here are:

(a) $-1.22 \pm .10$ percent $\Delta k/k$, for reused control rods

(b) $+0.21 \pm .10$ percent $\Delta k/k$, for modified type control rods.

G. Equilibrium Xenon (Core 3)

The reactivity equivalent of equilibrium xenon may be expressed as (see p. 470 of Ref. 11):

$$\rho = - \frac{\gamma_I + \gamma_X}{\nu \, p \, \varepsilon} - \frac{\phi_t}{\phi_t + \phi_x}$$

where:

γ_I = yield of I-135 (atoms/fission) from thermal fission
γ_X = yield of Xe-135 (atoms/fission) from thermal fission
ν = neutrons/fission
ρ = resonance escape probability
ε = fast fission factor
ϕ_t = thermal flux
ϕ_x = (decay constant for Xe-135)/(σ_{abs} for Xe-135)

To find $\bar{\nu}$ (the average number of neutrons released per fission), fissions in the three fissioning elements present must be considered: U-235, Pu-239, and Pu-241. Now,

$$\bar{\nu} = \sum_i Pi \, \nu_i$$

49

where P_i is the probability of fission in element i and ν_i is the number of neutrons per fission of element i. Further,

$$P_i = \frac{\Sigma \; fi}{\sum_j \Sigma \; fj}$$

where $\bar{\Sigma} fj$ is the core average macroscopic fission cross-section for element j. Namely,

$$\bar{\Sigma}_{fj} = \bar{N}_j \; \sigma_{fj}$$

where $\bar{N}_j$ is the core average number density of element J and σ_{fj} is the microscopic fission cross-section of element j. In turn,

$$\bar{N}_j = \frac{\sum_k N_j^k \; A^k}{\sum_k A^k}$$

where N_j^k is the number density of element j in composition k and A^k is the cross-sectional area of composition k. Assembling all these average quantities, one obtains the following equation for $\bar{\nu}$ for use in the equilibrium xenon equation:

$$\bar{\nu} = \frac{\sum_{i=1}^{3} \sum_{k=1}^{8} \nu_i \sigma_{fi} N_i^k A^k}{\sum_{i=1}^{3} \sum_{k=1}^{8} \sigma_{fi} N_i^k A^k}$$

where i is the element index ($i=1$ for U-235, $i=2$ for Pu-239, $i=3$ for Pu-241) and k is the composition index (in the quarter-core representation, there are 8 fuel compositions). For example, in the case of two fissionable elements distributed in two compositions:

$$\bar{\nu} = \frac{\nu_1 \sigma_{f1} \; (N_1^1 A^1 + N_1^2 A^2) + \nu_2 \; \sigma_{f2} \; (N_2^1 A^1 + N_2^2 A^2)}{\sigma_{f1} \; (N_1^1 A^1 + N_1^2 A^2) + \sigma_{f2} \; (N_2^1 A^1 + N_2^2 A^2)}$$

Using LEOPARD obtained cross-sections and the number densities and composition areas obtained from TURBO* one calculates the following value:

$$\bar{\nu} = 2.456$$

The fast fission factor may be obtained from a correlation presented in Ref 11 (p. 238):

$$\epsilon = \frac{1 + 0.987 \; (V_u/V_w)}{1 + 0.805 \; (V_u/V_w)}$$

50

where V_u/V_w is the uranium-water volume ratio, given to be 0.4392 by a LEOPARD calculation. This yields for the fast fission factor:

$$\epsilon = 1.059$$

LEOPARD also yields the value for the thermal flux ϕ_t, the Xe-135 absorption cross-section, and the resonance escape probability:

$$\phi_t = 1.0918 \times 10^{13} \text{ n/cm}^2\text{sec}$$

$$\sigma_{ax} = 2.7574 \times 10^6 \text{ barns}$$

$$p = .07559$$

Taking $\lambda_x = 2.09 \times 10^{-5}$ sec^{-1}, $\gamma_x = .003$, and $\gamma_I = .061$ one calculates the reactivity contribution of equilibrium xenon to be:

$$\rho = - \frac{.061 + .003}{(2.456)\ (.7559)\ (1.059)} \times \frac{1.0918 \times 10^{13}}{(1.0918 + .75795) \times 10^{13}}$$

$$= - 1.92\%$$

Thus the reactivity contribution of equilibrium xenon is - $2.74 (for $\beta_{eff} = .007015$, calculated in Section VI).

H. Radial Power Distributions (Core 3)

A parameter of major interest during power operation of a reactor is the ratio of maximum power density at any point within the core to the core average. The knowledge of this parameter (peaking factor) is important in reactor operations since limitations of the materials in the core serve to limit the energy output at a point. The maximum power density can be obtained by multiplying the average power density of the core times the peaking factor. To minimize the core total energy output without destroying the structural integrity of the core at the hottest point, one has to have an accurate knowledge of the peaking factors at all times during core life.

The x-y calculations done for MH-1A Core 3 with TURBO* give the radial power distributions as an output. The code computes and prints the power at each point in the reactor in a graphic form. The power at a point is averaged over the fuel quadrant at that point and normalized by the total power integrated over the fuel regions of the reactor. A fuel quadrant is defined as one for which Σ_f is nonzero for at least one group.

Thus, P_{ij} = power at the point $(i,j) = \dfrac{P^1_{ij}}{SpdA/SdA}$

$$
P^1_{ij} = \frac{\sum\limits_{g=1}^{4} \sum\limits_{q=1}^{4} (k \, \Sigma_f)^g \, q(i,j) \, \phi^g \,(i,j)}{\sum\limits_{q=1}^{4} \eta_q}
$$

q = quadrant about point (i,j)

g = number of energy group

k = energy produced for fission neutron

ϕ = neutron flux

Σ_f = fission cross-section

η_q = 1 if the composition in quadrant is fuel, and is zero for nonfuel quadrants.

The radial power distributions at 490°F are shown in Figure V-7. The values presented are normalized power density averaged over a fuel assembly. The local peaking effect for the central fuel assembly is shown in Figure V-8. The radial peaking reaches a maximum near the source element at the center of the core. This value is found to be 1.82 for MH-1A Core 3 with the reuse of the control rod followers. This value has changed from 1.68 predicted for Core 1 in reference 13. Thus, there is an increase of about 9 percent in the radial peaking factor. It should be pointed out that use of burnable poison in the inner control rod followers shall contribute a great deal towards power flattening. However, use of this poison in the outer control rod followers may not be that effective. Also it should be pointed out that the expected core behavior (to have the power distribution shift outward with each shuffle as per reference 13) has not been observed in our analysis. On the contrary, the inner fuel assemblies of Core 3 produce more power than the outer ones. This is shown in Table XXIII.

The reasons for the increase in the radial peaking factors in Core 3 may be the following ones.

MH-1A Core 3 is analyzed and found to be more reactive than the previous two cores. This is due to the fact that Core 2 is analyzed to have a shorter lifetime. The outer elements of Core 2 are depleted to a lesser degree to increase the average enrichment of Core 3.

The poisoned shim rods produce localized effects. However, collectively they do cause a slight increase in the radial power peaking.

A_4 1.045	A_5 .66	
B_4 1.556	B_5 1.21	B_6 .635
C_4 1.76	C_5 1.45	C_6 .93

FIG. V-7 QUARTER CORE RADIAL POWER DISTRIBUTION (CORE 3)
(reused borated followers)

53

								1.65	1.66
1.45	1.59	1.63	1.64	1.65	1.65	1.66	1.67	1.66	1.64
1.46	1.61	1.64	1.64	1.67	1.67	1.68	1.68	1.67	1.66
1.51	1.62	1.65	1.65	1.67	1.68	1.69	1.69	1.68	1.66
1.58	1.68	1.69	1.69	1.70	1.70	1.70	1.70	1.69	1.68
1.65	1.69	1.71	1.71	1.71	1.71	1.72	1.70	1.68	1.67
1.70	1.70	1.72	1.72	1.72	1.72	1.72	1.69	1.68	1.66
1.72	1.59	1.72	1.72	1.72	1.72	1.71	1.63	1.68	1.64
1.75	1.70	1.72	1.72	1.72	1.71	1.70	1.67	1.65	1.61
1.79	1.71	1.72	1.71	1.70	1.70	1.65	1.61	1.61	1.60
1.80	1.73	1.69	1.68	1.67	1.66	1.64	1.59	1.54	1.50
1.72	1.72								

FIG V - 8

RADIAL POWER DISTRIBUTION FOR CENTERFUEL
ASSEMBLY.   EACH FUEL PIN REPRESENTED.

54

The use of Type 1 modified control rods instead of reusing the depleted control rod followers will certainly increase the radial peaking factor to a still higher value.

Furthermore, Core 3 being more reactive, requires the control rod being inserted into the core to a greater extent than Core 2. This tends to give a lower value for the critical bank position with an increase in the axial peaking factor. The saving feature is that the peaking factors will decrease over the lifetime of Core 3.

TABLE XXIII

Fractional Power Production

MH-1A	Core 1	Core 2	Core 3
Inner elements	.6375	.6432	.650
Outer element	.3625	.3568	.350

I. Axial Calculations (Core 3)

The axial calculations consisted of determining the 12 rod bank integral and differential worths, the 12 rod bank critical positions, the axial power distributions and the peak-to-average power ratio at critical conditions for both BOL cold (100°F) and operating conditions (490°F). The complete analysis required the use of five computer codes. LEOPARD generated the microscopic cross-section input for 2D (spatially) reactivity calculations with TURBO*. TURBO* gives as output the value of group fluxes, the macroscopic cross-sections, and areas for all the different regions in the core. This output information was utilized in an inhouse computer code HOMOG to generate the spatially averaged cross-sections. This information was necessary as input for the one dimensional code CNCR-2. CNCR-2 solves the one dimensional multigroup diffusion equations using a standard finite difference source iteration scheme. The reactor was divided into four regions presented in Table XXIV for the one-dimensional CNCR-2 calculation.

Transverse leakage was accounted for by inputting a transverse buckling. A total of 108 mesh points were used. The reflector regions were each represented by eight mesh points with the rodded and unrodded

55

core regions containing the remainder. To simplify the input t>
CNCR-2, only macroscopic data was used. This resulted in some error
regarding the axial power distributions and peak-to-average power ratios
determined by CNCR-2. To correct the error, another inhouse code called
PEAK was used. Its use is described in detail in the section on
axial power distributions.

<div align="center">TABLE XXIV</div>

<div align="center">Region Description - - Axial Calculation</div>

Composition	Description
1	Water + stainless steel as reflector
2	Rodded core
3	Unrodded core
4	Water + stainless steel as reflector

The regions are pictorially depicted in figure V-9.

1. Cross-Section Input

a. Water + stainless steel reflector: These cross-sections
were obtained by simply area weighting the pure water and pure stain-
less steel cross-sections generated by LEOPARD.

b. Unrodded core: These were calculated using TURBO* and
an inhouse code called HOMOG. Twenty-one region macroscopic cross-
sections were generated from TURBO* (xy) runs. HOMOG averaged these
twenty-one region cross-sections by conserving reactions per unit
core height using the following relation:

$$\Sigma_g^k = \frac{\sum_{i=1}^{k} \Sigma_{ig} \phi_{ig} A_i}{\sum_{i=1} \phi_{ig} A_i}$$

k = type of cross-section indicated
g = no. of energy group
i = no. of region
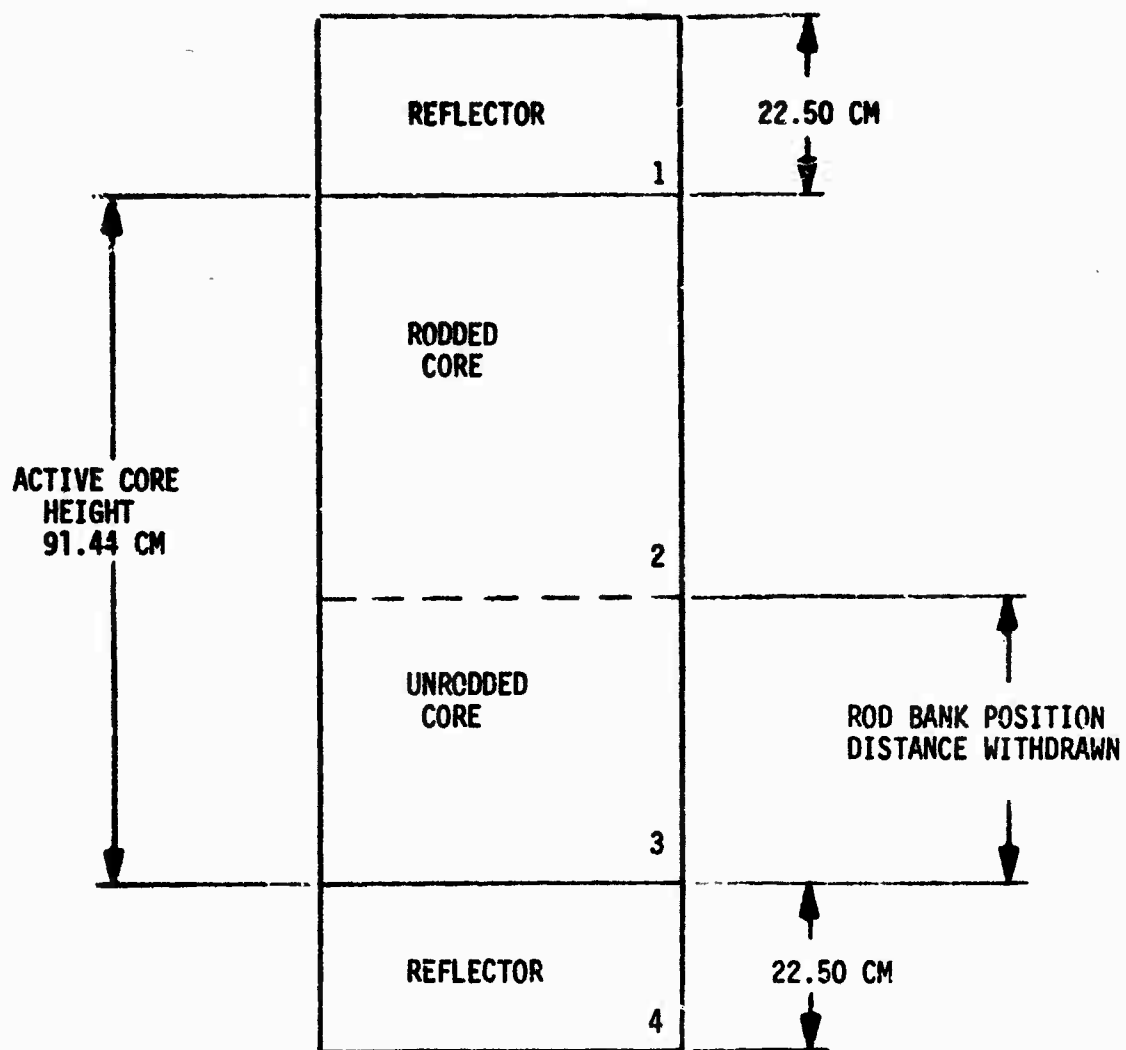Σ = cross-section
ϕ = flux
A = area

FIG V-9 DEPICTION OF REGIONS
USED IN AXIAL CALCULATIONS

c. Rodded core: These cross-sections were calculated in the same manner as those in the unrodded core.

2. Rod Rank Worth and Critical Bank Position

The 12 rod bank position was simulated by moving the boundary between the unrodded and rodded regions of the core. The differential rod bank worth was calculated using:

$$\frac{\Delta \rho}{\Delta L}(x) = \frac{K(x+\Delta x/2) - K(x - \Delta x/2)}{K(x+\Delta x/2) \quad K(x-\Delta x/2)} \quad \frac{1}{\Delta x}$$

$\frac{\Delta \rho}{\Delta L}(x)$ = differential rod bank worth with the rod bank withdrawn a distance x.

$K(x)$ = effective multiplication factor with the rod bank withdrawn a distance x.

The integral rod bank worth was calculated using:

$$\rho(x) = \frac{K(X) - K(X=0)}{K(X)K(X=0)}$$

$\rho(x)$ = integral rod bank worth with the rod bank withdrawn a distance X.

$K(X=0)$ = effective multiplication factor with the rod bank completely inserted.

Figures V-10 and V-11 give integral and differential rod bank worth as a function of rod bank position (inches withdrawn) for both hot (490°F) and cold (100°F) BOL conditions. The critical bank positions under both hot and cold conditions at BOL were determined by systematically varying the rod bank position until an effective multiplication factor of unity was obtained. As criticality was approached, the maximum bank movement per run was 1 cm. The bank position at criticality was then determined by a linear extrapolation. Critical bank positions of 11.2 and 5.25 inches were obtained for the hot and cold cases respectively.

J. Axial Power Distribution

Axial power distributions were obtained for both hot and cold BOL critical conditions. Because macroscopic cross-sections were input to CNCR-2, the rodded region of the core had to be represented by Pu^{239}. This resulted in both an incorrect power distribution and axial power peaking factor due to the difference in amounts of energy produced per fission in U^{235} and Pu^{239}. To account for this difference, an inhouse code entitled PEAK was used to correct the power distributions

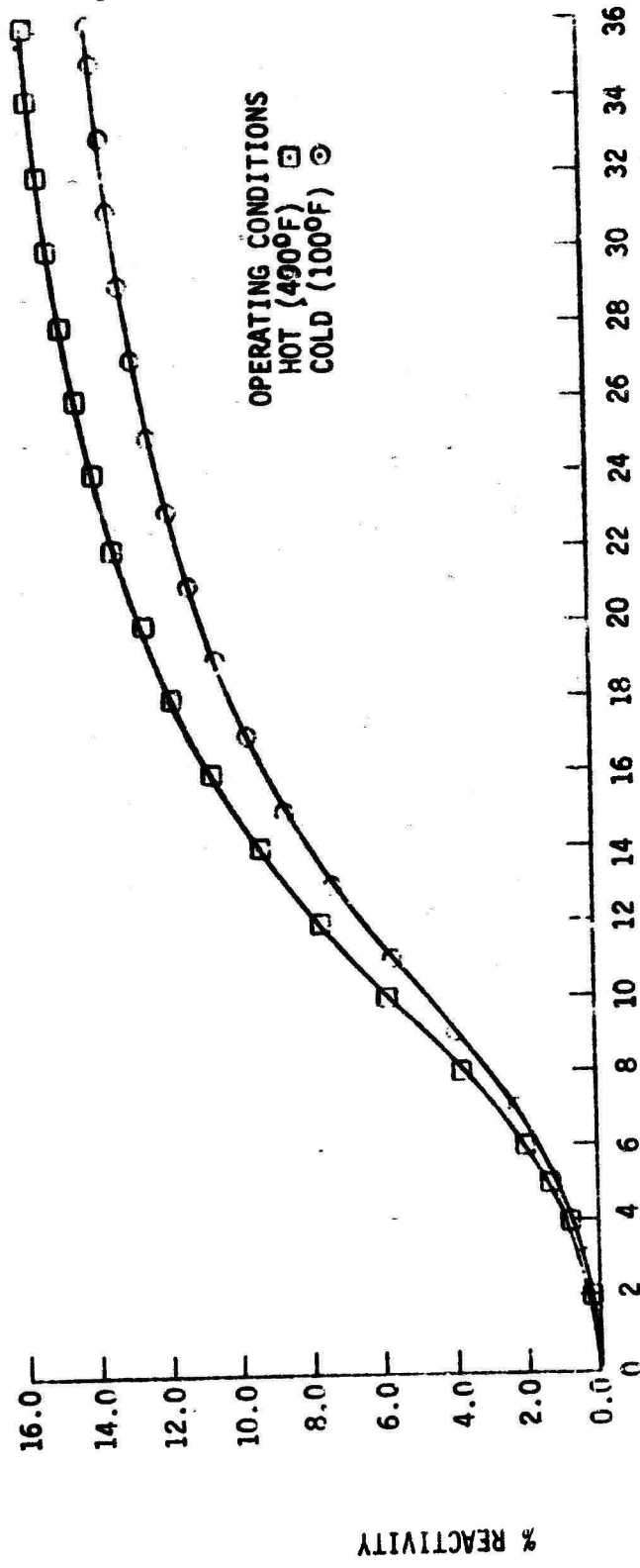58

MH-1A CORE III BOL
ROD BANK INTEGRAL WORTH

OPERATING CONDITIONS
HOT (490°F) ☐
COLD (100°F) ⊙

FIG V-10   ROD BANK POSITION, INCHES WITHDRAWN

% REACTIVITY

MH-1A CORE III BOL

ROD BANK DIFFERENTIAL WORTH

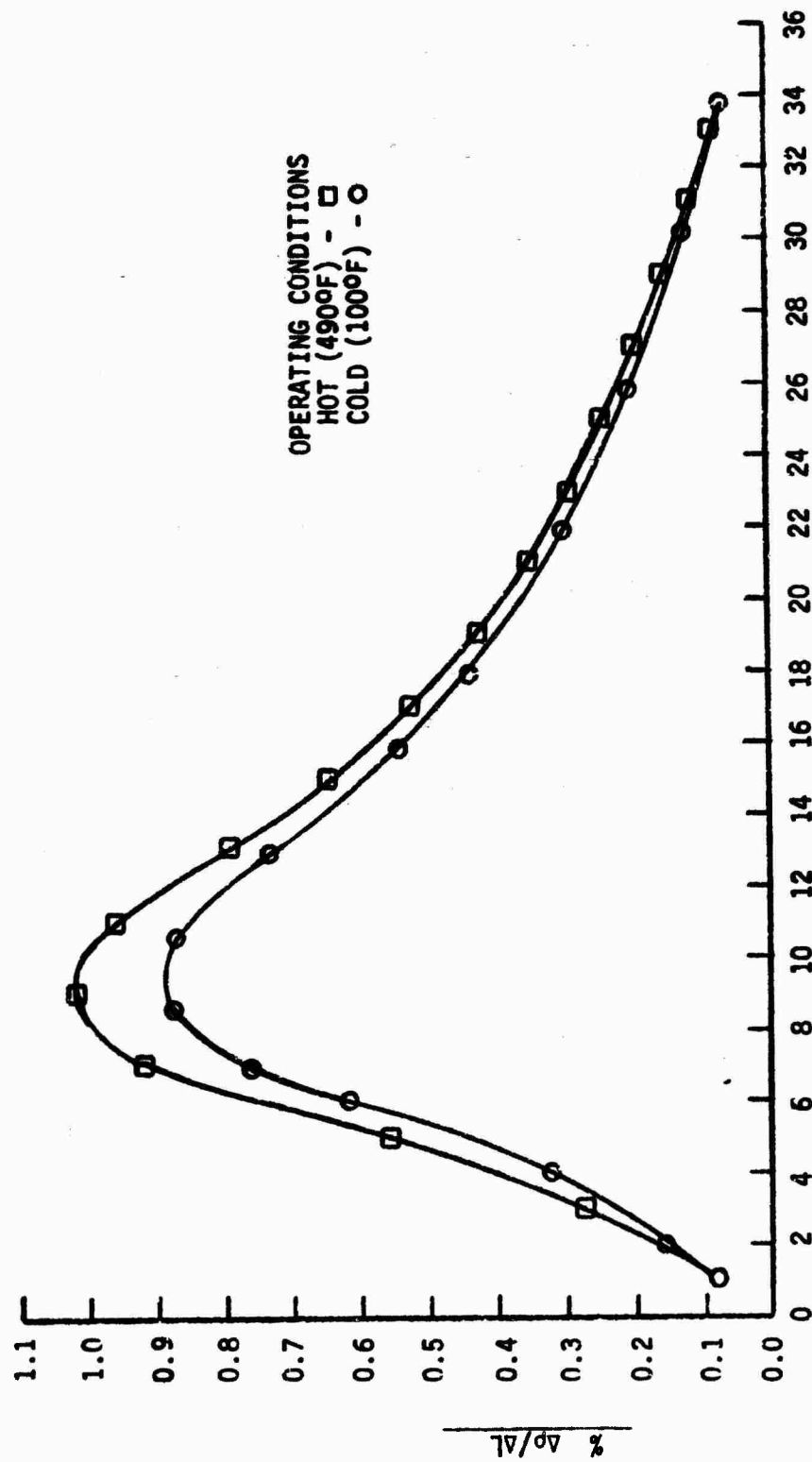
FIG V-11 ROD BANK DIFFERENTIAL WORTH

by adjusting the CNCR-2 power distributions. Under hot critical conditions a peak-to-average power ratio of 2.04 located at 7.7 inches from the core base was obtained. A peak-to-average power ratio of 1.30 located 15.0 inches from the core base resulted under cold critical conditions. The normalized power distributions under both operating conditions are presented in Figure V-12.

The effect of rod bank position on peak-to-average power ratio was briefly investigated. Figure V-13 illustrates this effect. The solid curve represents a least squares 3rd order polynomial fit. As can be noted from the figure, the rod bank position rather than the operating condition had a greater effect on the peak-to-average power ratio.

The axial peaking factor at BOL for Core 3 under operating conditions (490°F) is 2.04. This value is higher than the 1.91 for Core 1 (reported in ref. 13). Thus, there is an increase of about 6 percent in the axial peaking factor. The reason for this increase is the fact that Core 3 is more reactive, which necessitates the rods to be further inserted. The use of Type I modified control rods will probably increase the axial peaking factor by more than this 6 percent. A plot of the axial peak-to-average power ratio at critical for Core 3 is presented in Figure V-14.

The total peaking factor for Core 3 broken down into its individual contributions is:

Radial Peaking Factor	1.82
Axial Peaking Factor	2.04
Engineering Factor (ac- counting for local uncertainties -see section V.M.)	1.073

Thus the total peaking factor for Core 3 is 3.984. For purposes of comparison, for Core 2 its value was 3.40.

K. Temperature Coefficient (Core 3)

An increase in temperature causes a decrease in the reactivity of the core due to decrease in moderation with decreased water density. There is also a contribution to the change in reactivity through the Doppler effect for the fuel.

The moderator temperature coefficient is defined as the change in reactivity per degree change in moderator. The influence of fuel temperature was eliminated by maintaining the fuel temperatures identical to the moderator temperature in evaluating the cross-sections at different temperature of interest with LEOPARD. The LEOPARD runs were made at 100°F, 200°F, 300°F, 400°F, and 490°F to obtain the cross-

61

FIG V-12 MH-1A CORE III BOL CRITICAL

NORMALIZED POWER DISTRIBUTION

OPERATING CONDITIONS

HOT (490°F) - ▣
COLD (100°F) - ⊙

INCHES FROM CORE BASE

POWER/AVERAGE POWER

FIG V-13 MH-1A CORE 1V BOL
PEAK TO AVERAGE POWER RATIOS

OPERATING CONDITIONS
HOT (490°F) - ☐
COLD (100°F) - ○

LEAST SQUARES FIT

ROD BANK POSITION, INCHES WITHDRAWN
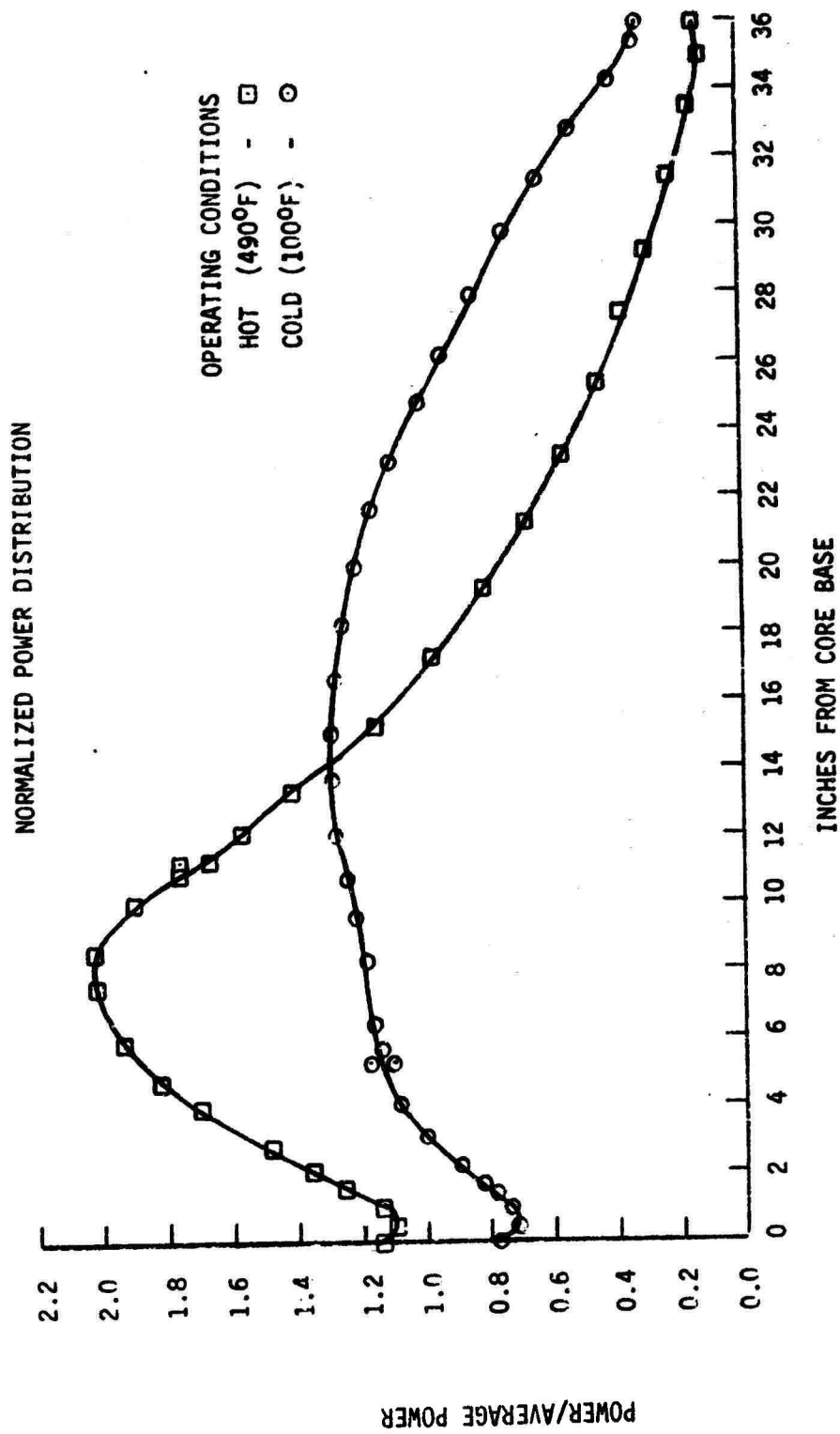
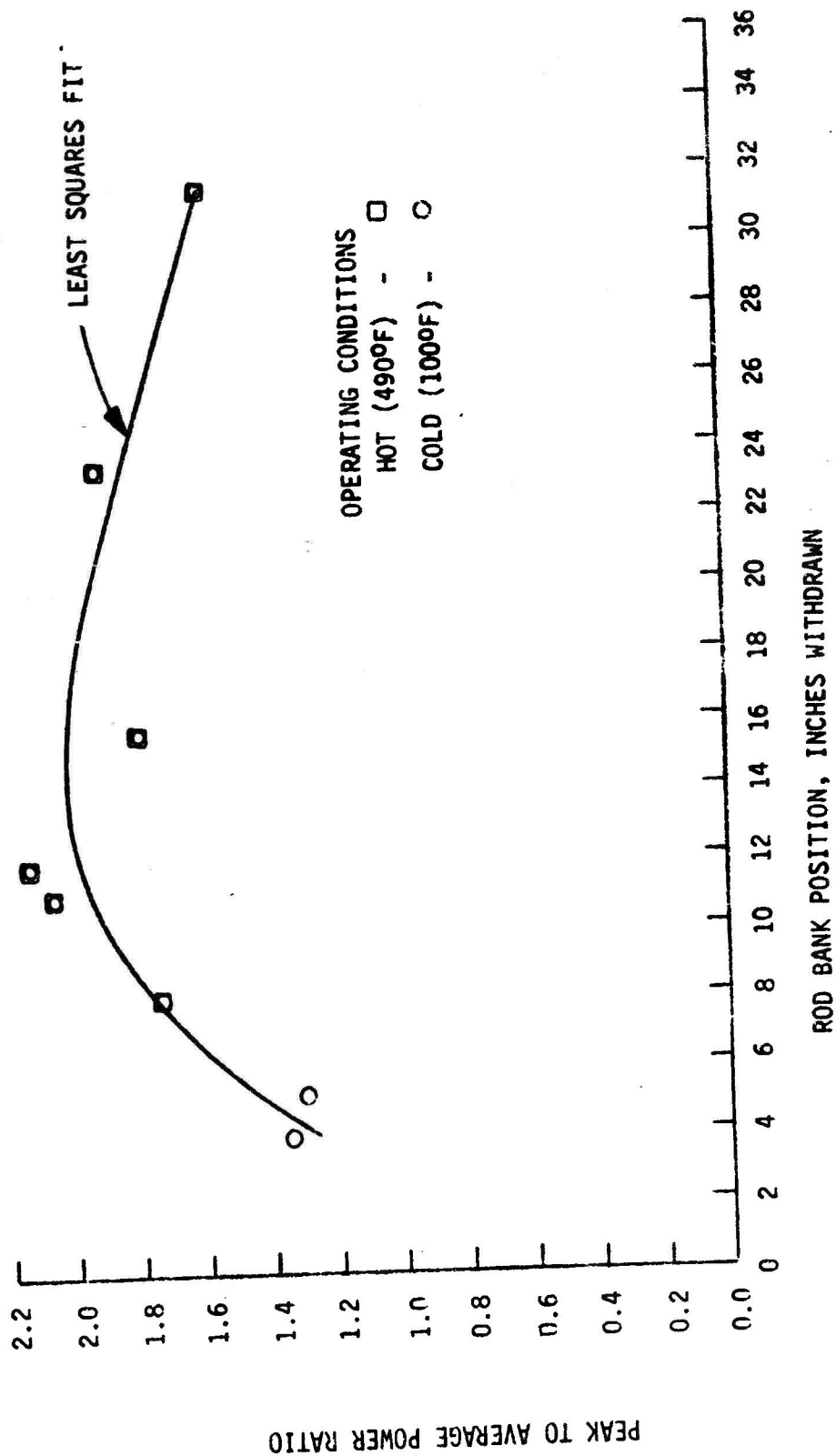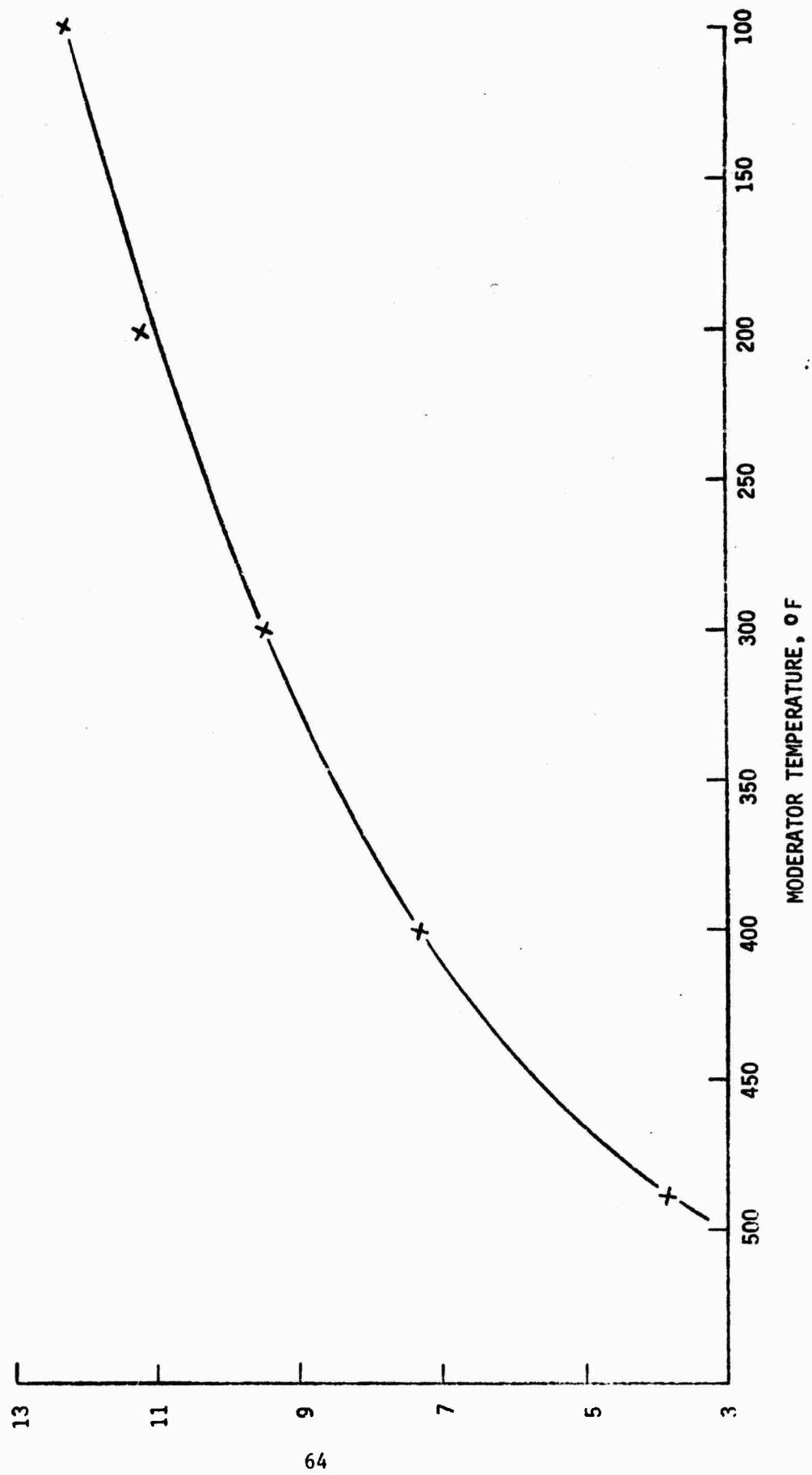PEAK TO AVERAGE POWER RATIO

FIG V-14 MH-1A CORE REACTIVITY VS. TEMPERATURE

MODERATOR TEMPERATURE, °F

64

sections at these temperatures. LEOPARD gives as output the value for the effective multiplication factor of the core for these temperatures. These were utilized as a first attempt to calculate the temperature coefficient.

The values of $\frac{(k_{eff} - 1)}{k_{eff}}$ versus temperature were plotted. This curve was utilized to obtain $\frac{d\rho}{dT}$ at specific temperature by drawing slopes on the curve. The evaluated values were then fitted to an expression of the form

$$\frac{d\rho}{dT} = a\,T + b$$

a, b being fitted parameters.
ρ = reactivity, cents
T = Temperature of moderator, °F.

The temperature defect, defined as the change in reactivity of the core from cold to hot, was obtained from TURBO* (x,y) calculations. The presence of absorbers (control rods, poison shims, borated followers) does influence the overall negative contribution to the temperature effects. It is necessary to do the calculations with the rods at critical bank position.

The above statement is very clear when one calculates the temperature defect from TURBO* run for the cases with rods completely inserted and completely withdrawn. The temperature defect with rods-in cases are higher than that calculated with rods-out conditions.

TABLE XXV

Temperature Defect

		k_{eff} (calculated)	%Δ k
Calculation 1.	TURBO, rods out, cold (100°F)	1.123	+10.95
	TURBO, rods out, hot (490°F)	1.058	+ 5.48
Calculation 2.	TURBO, rods in, cold (100°F)	.952	- 5.04
	TURBO, rods in, hot (490°F)	.884	-13.12

65

FIG V-15 TEMPERATURE COEFFICIENT AS A FUNCTION OF MODERATOR TEMPERATURE

$$-\frac{d\rho}{dT} = /005601\ T + .1756$$

NEGATIVE TEMPERATURE COEFFICIENT, $\cancel{c}$/°F

MODERATOR TEMPERATURE, °F
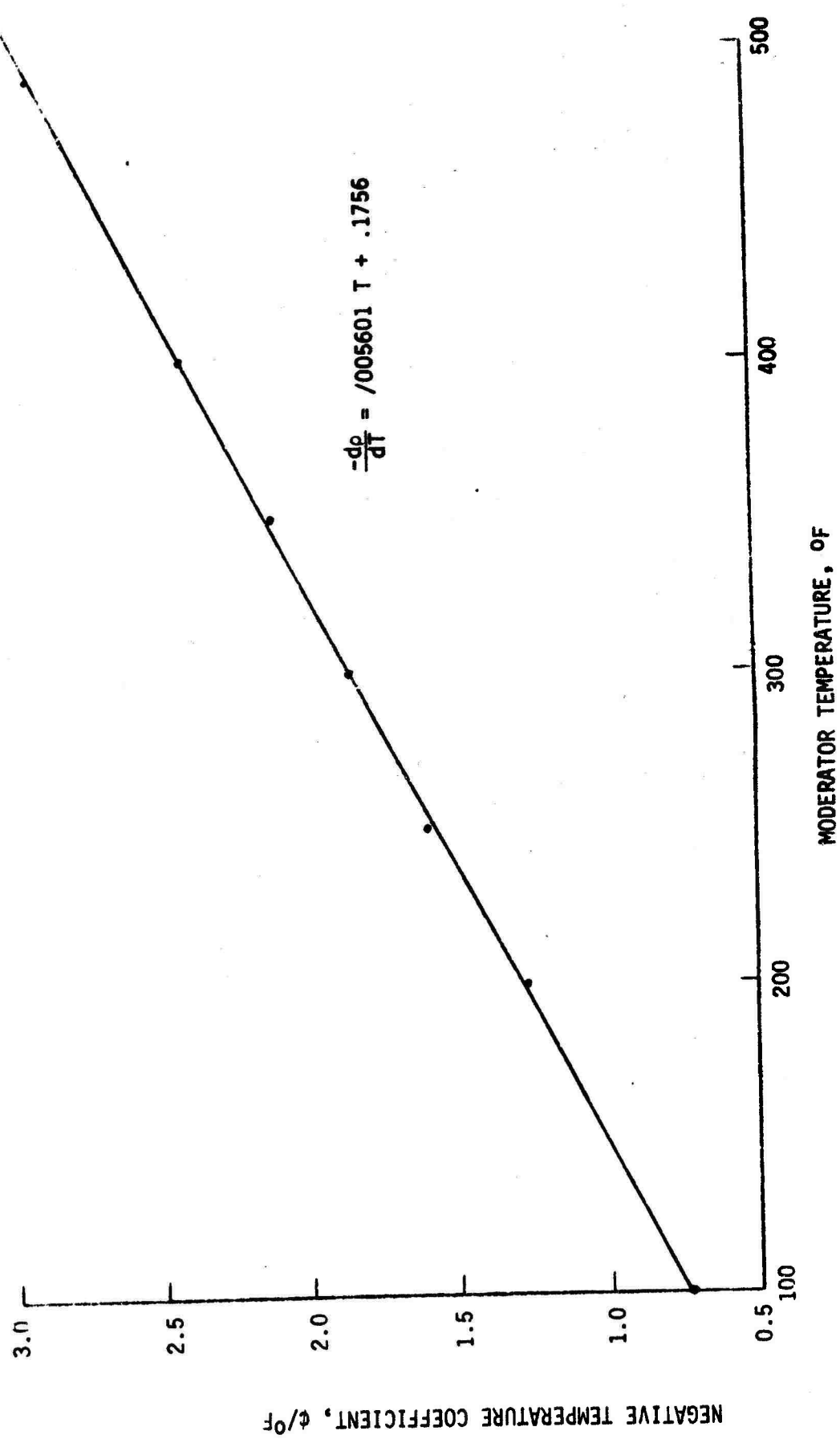
The temperature defect from calculation 1 is thus -5.47 percent Δk and that from calculation 2 is -8.08 percent Δk. The measured value for Core 2 is -6.47 percent Δk (Ref 12) and prediction for Core 1 was -4.8 percent Δk (Ref 13). The measured value for Core 2 was from a temperature range of 68°F and the value calculated with rods in is from 100° to 490°F.

Core 3 is more reactive than core 2. This requires the rod to be inserted more for maintaining criticality. This suggests that the defect should be evaluated with the rods in, although one would evaluate with rods at a near critical position.

TABLE XXVI

Negative Temperature Coefficient

Temperature. °F	Cents /°F
100	.74
200	1.296
250	1.58
300	1.86
350	2.14
400	2.42
490	2.92

L. Prompt and Delayed Neutron Characteristics (Core 3)

The prompt neutron lifetime was calculated at full power conditions during the core life. The values were obtained as part of the output in the LEOPARD code. It was noticed that the prompt neutron lifetime is not very sensitive to burn up.

TABLE XXVII

Prompt Neutron Lifetime versus Burn-up

Burn up MWD	Prompt Neutron lifetime (μSec)
0	13.01
27.5	12.73
275.0	12.65
687.5	12.58
1375.0	12.46
2750.0	12.32

67

Delayed Neutron Characteristics. The reactivity of the core is determined by measuring a stable period following a small perturbation and solving the in-hour equation. The in-hour equation is derived wherein both prompt and delayed neutrons are included.

$$\rho = \frac{\ell^*}{T} + \sum_{i=1}^{6} \frac{\beta_{i_{eff}}}{1 + \lambda_i T}$$

ℓ^* = Prompt neutron lifetime

T = The reactor period (asymptotic value)

$\beta_{i_{eff}}$ = Effective delayed neutron fraction

λ_i = Decay constant for the precursors.

The first term can be ignored as $T >> \ell^*$.

The delayed neutrons are born with lower energies than the prompt ones. This contributes lower leakage probabilities for delayed neutrons, or in other words, the weight delayed neutron fraction, β_i, should be multiplied by an importance factor or effectiveness factor to obtain $\beta_{i_{eff}}$.

It is assumed that this importance factor has the same value for all the delayed groups. The delayed neutron data were computed by utilizing information on fission fraction for various isotopes from the TURBO* code and fast fission and slow fission factors from the LEOPARD code.

The average thermal neutron flux is calculated to be 875×10^{12} n/cm^{2}sec at BOL operating conditions.

TABLE XXVIII

Delayed Neutron Data

1. Shuffled Core, (Core 3)			
Fission	**Break-down**	**Fraction**	
U-235	U-238	Pu $\binom{239}{241}$	
.8688	.0640	.0672	

Absolute Yield – Total

U-235	U-238	Pu 239-241	Total
2.1598	.1680	.1960	2.5238

Absolute Yield – Delayed %

U-235	U-238	Pu 239-241	Total	Group
.0476	.0035	.0014	.0525	1
.3016	.0366	.0126	.3508	2
.2693	.0421	.0092	.3206	3
.5528	.1025	.0130	.6683	4
.1649	.0561	.0041	.2251	5
.0521	.0199	.0023	.0743	6
1.3883	.2607	.0426	1.6916	

Decay Constants

U-235	U-238	Pu 239-241	Total	Group
.01131	.00091	.00034	.01256	1
.02659	.00332	.00105	.03096	2
.09408	.01861	.00362	.11631	3
.25086	.05511	.00658	.31255	4
.86543	.36882	.01831	1.25256	5
2.28000	1.08122	.06728	3.4285	6

TABLE XXVIII (cont'd)

δ Fraction Z β	Effective β	Group
.0210	.0217	1
.1391	.1439	2
.1271	.1328	3
.2654	.2770	4
.0910	.0951	5
.0296	.0310	6
.6732	.7015	

Effectiveness Factor ≈ 1.042   (Ref 13)

M. Local Uncertainties

The uncertainties that should be included to influence the peaking factors are inlet flow maldistribution, pellet diameter variations, enrichment variations, uranium density variations, etc. The appropriate value for use in the MH-1A Core 3 can be calculated with the following information:

Enrichment variation, %	± 4
Density of fuel elements, %	± 3
Variation in pellet size loading %	± 5

The above numbers are based on engineering judgment. The contribution to the peaking factor value combining these variations is computed to be 1.073. The value does not take into account flow maldistributions.

70

VI. ANALYSIS OF THE SHUFFLED CORE
AFTER EXTENDED DEPLETION OF CORE 2.

A. Introduction -- Core 3A

As discussed earlier, if Core 2 were shuffled and refueled after
241 full power days, the resulting new core would not be able to meet
the stuck rod shut-down margin requirement of -1 percent $\Delta k/k$ with
use of the modified type control rods. Thus, the decision was made to
extend the analytical TURBO* depletion of Core 2 to 300 full power
days, and then perform the shuffle and reloading. The resulting core
is called Core 3A to distinguish it from the core resulting from the
shuffle and refueling of the 241 full power days Core 2.

It is assumed that Core 3A will represent the third core to be
installed in the MH-1A, and the requisite BOL calculations and depletion
results follow for this specific core.

B. Core 3A, TURBO* BOL Calculations

The BOL calculations for Core 3A were made with several refinements
in technique as compared to earlier calculations: Both MND and Wigner-
Wilkens (WW) thermal group cross-section sets were considered; buckling
changes were considered; temperature dependent absorber cross-section
sets were used. Table XXIX presents the absorber region constants
used in Core 3A calculations.

71

TABLE XXIX

Core 3A BOL Absorber Constants

Control Rod:

	Hot			Cold		
Group	Σtr	Σa	Σr	Σtr	Σa	Σr
1	.2064	.2837x10^{-2}	.04131	.2087	.20289x10^{-2}	.04131
2	.3684	.01293	.2606x10^{-2}	.3732	.01295	.2660x10^{-2}
3	.4880	.4015	1.276x10^{-3}	.5113	.4190	.1298x10^{-3}
4-MND	15.23	5.509	–	21.44	4.599	–
4-WW	2?.06	2.876	–	24.90	2.895	–

Shim Rod:

	Hot			Cold		
Group	Σtr	Σa	Σr	Σtr	Σa	Σr
1	.2064	.3516x10^{-3}	.03934	.2087	.3545x10^{-3}	.03981
2	.3684	.9186x10^{-3}	.2606x10^{-2}	.3732	.9174x10^{-3}	.2660x10^{-2}
3	.9236	.05744	.1276x10^{-3}	.9344	.05982	.1298x10^{-3}
4-MND	.6195	1.343	–	.8176	1.264	–
4-WW	.9373	.7043	–	.9496	.7959	–

The Σ_a values are all from LEOPROD calculations while the Σ_{tr} values have been chosen from either the LEOPROD or the pure stainless steel values as detailed in the earlier discussion of the ratio criterion (Section V-B). All other cross-sections were obtained from LEOPARD calculations for Core 3A. Table XXX presents the TURBO* results for Core 3A.

72

TABLE XXX

Core 3A BOL TURBO* Results

Inner stuck rod, 100°F, MND:	k = 0.998971
Inner stuck rod, 100°F, WW:	k = 0.981365 (B^2 = .1031x10^{-2})*
Rods out, 100°F, MND:	k = 1.15223
Rods out, 100°F, WW:	k = 1.15247
Rods out, 490°F, MND:	k = 1.08601
Rods out, 490°F, WW:	k = 1.08600
Rods in, 100°F, MND:	k = 0.949988
Rods in, 100°F, WW:	k = 0.927918 (B^2 = .1031x10^{-2})*
Rods in, 100°F, WW:	k = 0.930665
Rods in, 490°F, MND:	k = 0.860551

* All other calculations with B^2 = .939x10^{-3}

One significant result is the sizable difference between the two k_{eff}'s for the stuck rod calculation. The k_{eff} obtained using the WW thermal group cross-section set indicates a stuck-rod shut-down margin of -1.90 percent $\Delta k/k$ while the result with the MND cross-section set is -0.103 percent $\Delta k/k$. This latter result for Core 3A is to be compared to the value of +0.21 percent $\Delta k/k$ obtained for Core 3.

The question arises: Which calculation, the one using the MND or the one using the WW set, is to be believed? The literature (p. 454 ff of Ref. 15) maintains that the WW set results is a better calculation of the multiplication constant, but due to the too large diffusion lengths which the WW model results in, the MND set represents more accurately the power peaking and depletion effects.

Since the quantity of interest in the stuck rod calculation is solely the value of k_{eff}, the WW set should be used in the calculation. Thus, the -1.90 percent $\Delta k/k$ shut-down margin meets the requirement of -1.0 percent $\Delta k/k$. In addition, the MND calculation also indicates the core is subcritical for a single stuck rod using the MND cross-section set (which Core 3 was not). This suggests that the stuck rod

shut-down requirement be prescribed more rigorously: That
the stuck rod shut-down margin calculated using the WW cross-section
set be at least -1 percent $\Delta k/k$, and that the core be subcritical
for an identical calculation with the MND cross-section set. Other-
wise, it is conceivable the core meets the -1 percent $\Delta k/k$ shut-down
margin in the WW calculation, yet has $k_{eff} > 1.0$ in the MND calculation.
The simultaneous presence of both criteria for Core 3A gives a con-
fidence in the core's safety in the one stuck rod configuration.

The effect of the two cross-section sets is further clarified
by the results of the rods-in and rods-out calculations presented in
Table XXX. The 490°F rods-out calculations for MND and WW cross-
section sets are identical. Similarly, the 100°F rods-out calculations
differ only slightly (the WW calculation yields a k_{eff} which is 0.00024
larger). On the contrary, the rods-in calculations indicate a major
difference due to the choice of cross-section set. Use of the WW set
yields a k_{eff} which is 0.019323 less than the MND value. This effect
is consistent with the result observed when the stuck rod calculation
was performed with the two sets. Thus, one concludes that it is the
representation of the control rods themselves which causes the major
difference between the MND and WW results. Assuming the WW result to
yield the better k_{eff} value, it is concluded that the MND thermal
group cross-section set yields a value of k_{eff} for the rods-in case
which is approximately 2.08 percent to large.

To observe the effect of buckling change, the rods-in case at
100°F with the WW set was run once with $B^2 = .939 \times 10^{-3}$ (the rods-out
hot B^2 value suggested by Ref. 13) and once with $B^2 = .1031 \times 10^{-2}$ (the
rods-in cold B^2 value suggested by Ref. 13) in order to observe the
effect of the buckling choice. From the results of Table XXX, it is
concluded that use of the improper buckling value causes k_{eff} to be
0.002747 too large when $B^2 = .939 \times 10^{-3}$ is used for the cold, rods-in
calculations. Table XXXI details the suggested buckling values for
various cases from Reference 13.

TABLE XXXI

Suggested Buckling Values

Rods In, Cold:	$B^2 = .001031$
Rods Out, Cold:	$B^2 = .000954$
Rods In, Hot:	$B^2 = .001016$
Rods Out, Hot:	$B^2 = .000939$

74

C. Temperature Defect and Other BOL Parameters

It is assumed that the additional depletion of Core 2 resulting in Core 3A will not change the overall system parameters (such as moderator temperature coefficient, prompt and delayed neutron characteristics, Doppler coefficient, and uncertainty factors) from those reported for Core 3 in Section V. However, it is recognized that the shut-down margins have to be recalculated for Core 3A in the light of the above comments on choice of the WW or MND cross-section sets.

Table XXXII presents the results for Core 3A based on the proper WW cross-section set.

TABLE XXXII

Quantities Based On BOL k_{eff} Calculations (WW)

Stuck rod shut-down margin:	-1.899% $\Delta k/k$
Temperature defect (from rods out):	5.311% $\Delta k/k$
Temperature defect (from rods in):	11.495% $\Delta k/k$
Shut-down margin (hot):	-19.263% $\Delta k/k$
Shut-down margin (cold):	-7.768% $\Delta k/k$
Excess reactivity (hot):	7.919% $\Delta k/k$
Excess reactivity (cold):	13.230% $\Delta k/k$

Note: Hot = 90°F moderator; Cold = 100°F moderator

In comparing these results for Core 3A to those of Core 3, it should be kept in mind that the control rods for the Core 3 calculations contained depleted followers, while those used in the Core 3A calculations contained stainless steel followers. For purposes of comparison: The MND value for the temperature defect found from the rods-in case is 10.941 percent $\Delta k/k$.

As in the case of Core 3, there is again observed a major difference between the temperature defects obtained from the rods-in and the rods-out cases. This may be explained by noting the following: With the control rods fully inserted, the flux is "pushed" out into the core periphery (i.e., into the reflector/moderator). Since the temperature

75

defect is primarily a moderator density effect, the rods-in case should result in a larger temperature defect due to the greater neutron importance in the region where the significant temperature effect occurs. This rationale is consistent with the result observed. Thus it is concluded that the temperature defect is a phenomenon which depends fairly strongly upon the control rod bank position.

D. Axial and Radial Calculations, and the Peaking Factors

The axial calculations were performed for Core 3A as explained above in Section V, I and J; thus only the results will be presented here, the procedures being discussed in the aforementioned sections.

Figures VI-1 through VI-3 present, respectively, the curves for the integral rod bank worth, the differential rod bank worth, and the critical normalized power distribution. From Figure VI-3 it is concluded that at 100°F, the maximum peak-to-average power ratio is 1.29 and is located 14.06 inches from the core base. At 490°F, the maximum peak-to-average power ratio is 1.96 and is located 7.44 inches from the core base. The cold critical bank position is found to be 4.243 inches withdrawn, while the hot critical bank position is found to be 10.603 inches withdrawn.

As expected, the critical bank positions were lower (i.e., less withdrawal) for Core 3A than for Core 3 because the control rods for Core 3 contained borated followers, while those for Core 3A were only stainless steel. In addition, the axial peaking factor for Core 3A is slightly less due to its greater burn-up in the shuffled fuel elements. Unexpectedly, however, there is noted the anomalous cross-over of the hot and cold worth curves. It is unclear if this is a meaningful physical effect since the degree of cross-over is approximately equal to the uncertainty of the calculation. Where the cross-over occurs, it may be more meaningful to simply consider the hot and cold worths to be approximately equal.

The radial power distribution was found, as before, with the TURBO* program. Figures VI-4 and VI-5 present the radial power distributions for the central fuel element (the worst case) for the rods-out and the rods-in cases, respectively. From the former, it is concluded that the maximum radial peaking factor is 1.92.

Table XXXIII details the peaking factor contributions for Core 3A which yield a total peaking factor of 4.04.

76

FIG VI-1 MH-1A CORE 3 A BOL ROD BANK

INTEGRAL WORTH

ROD BANK POSITION, INCHES WITHDRAWN

% REACTIVITY

OPERATING CONDITIONS

HOT (490°F) - ☐

COLD (100°F) - ◉

77
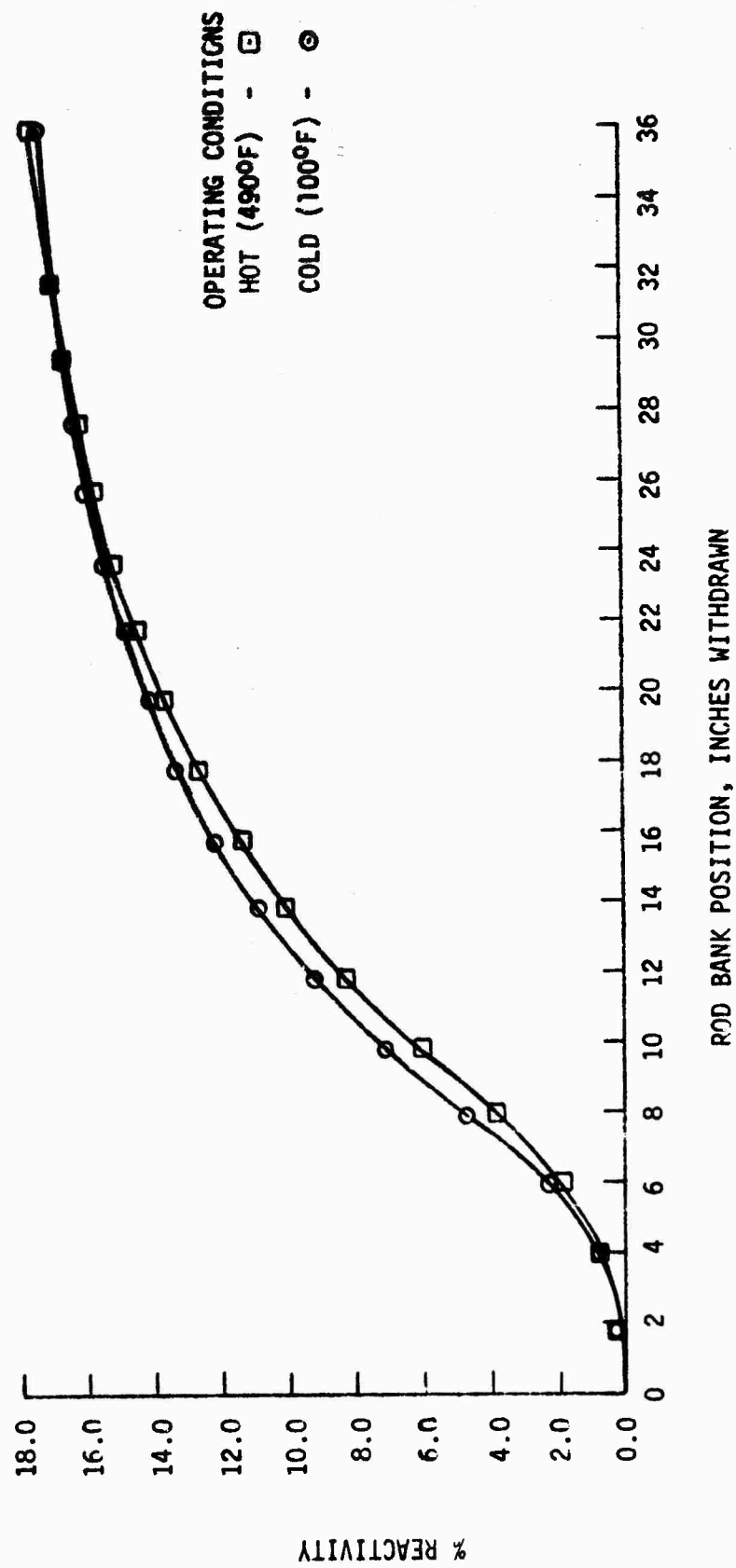
FIG VI-2 MH-1A CORE 3 A BOL ROD BANK

DIFFERENTIAL WORTH

OPERATING CONDITIONS
HOT (490°F) - □
COLD (100°F) - ○

ROD BANK POSITION, INCHES WITHDRAWN

% Δρ/ΔL
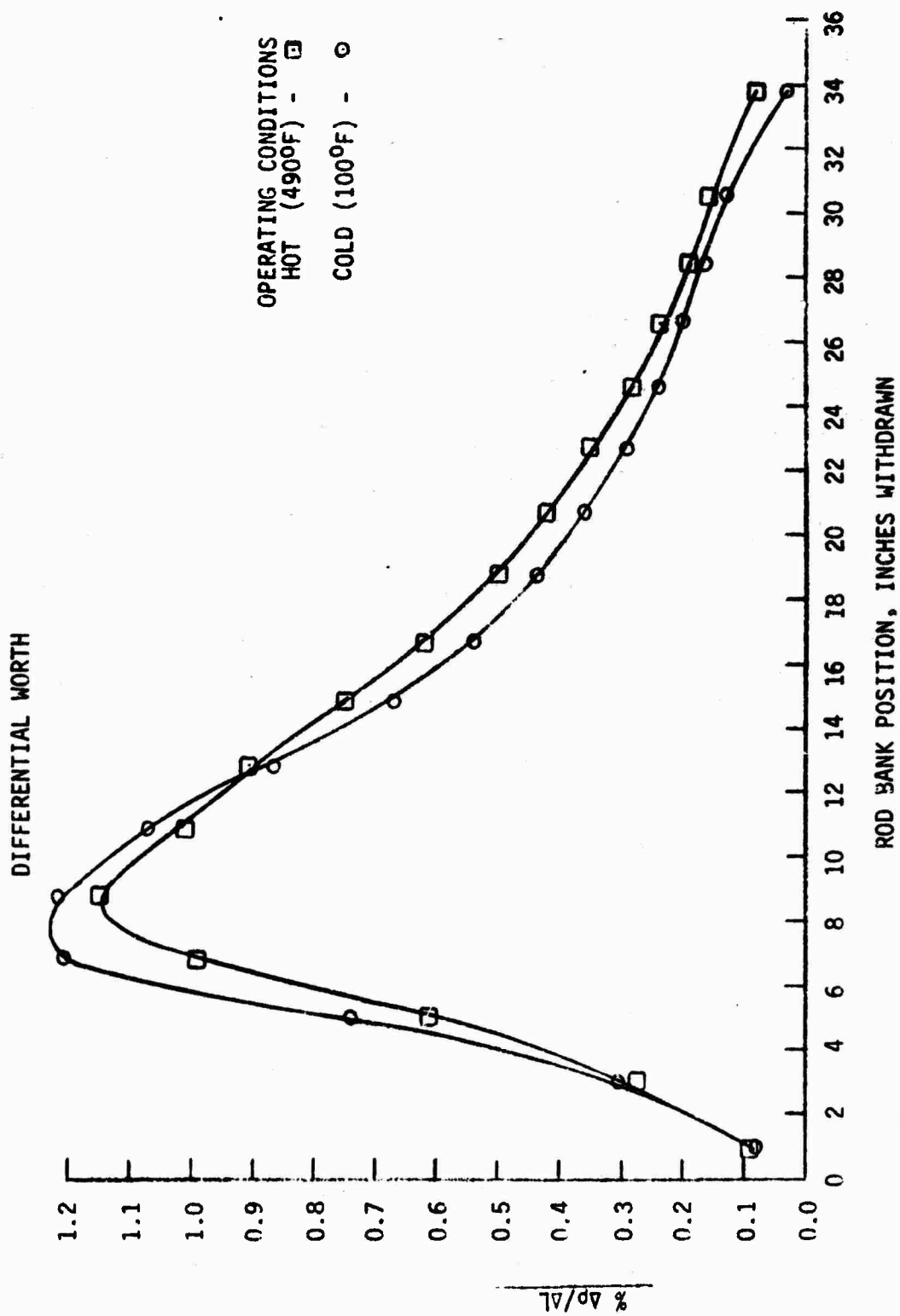
FIG VI-3 MH-1A CORE 3 A BOL CRITICAL

NORMALIZED POWER DISTRIBUTION (AXIAL)
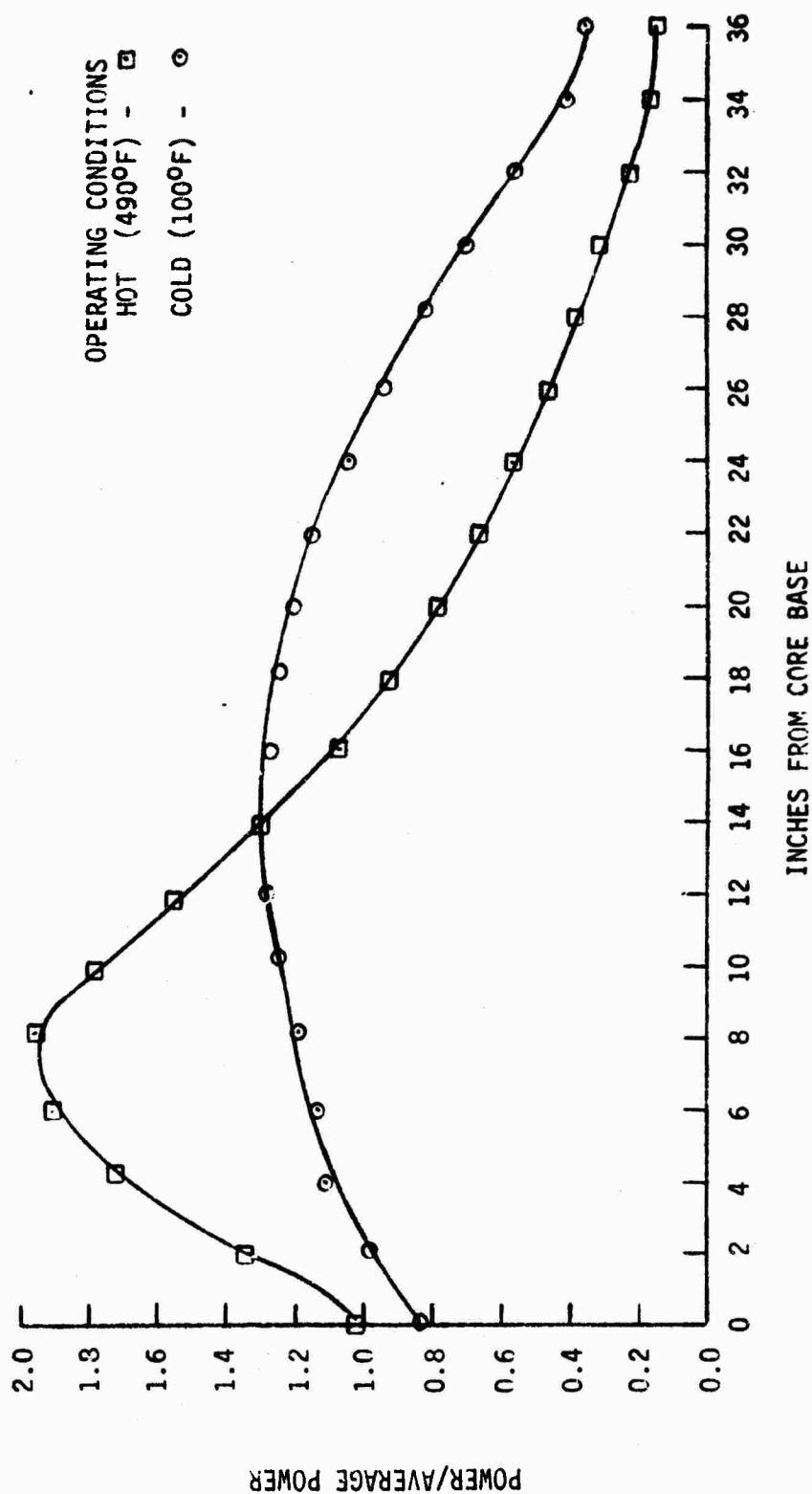
								1.51	1.21
1.92	1.77	1.76	1.75	1.73	1.70	1.66	1.64	1.60	1.33
1.81	1.61	1.60	1.59	1.57	1.55	1.52	1.52	1.51	1.58
1.81	1.61	1.59	1.58	1.57	1.55	1.52	1.51	1.51	1.62
1.81	1.60	1.58	1.58	1.57	1.54	1.52	1.51	1.51	1.63
1.80	1.59	1.58	1.58	1.56	1.53	1.52	1.52	1.52	1.64
1.805	1.59	1.59	1.58	1.56	1.53	1.53	1.53	1.53	1.67
1.80	1.59	1.59	1.58	1.56	1.54	1.53	1.53	1.53	1.68
1.78	1.59	1.59	1.58	1.56	1.54	1.53	1.53	1.54	1.69
1.76	1.60	1.59	1.58	1.57	1.55	1.53	1.54	1.54	1.69
1.45	1.66	1.68	1.68	1.68	1.67	1.64	1.65	1.65	1.68

Source | 1.22 | 1.65 |

FIG VI-4 MH-1A CORE 3A (RODS OUT)

RADIAL POWER DISTRIBUTION FOR CENTRAL
FUEL ASSEMBLY

80

								1.25	1.13
.78	..97	.99	1.00	1.06	1.10	1.18	1.23	1.28	1.23
.97	1.24	1.26	1.28	1.35	1.36	1.37	1.38	1.37	1.26
.98	1.26	1.29	1.31	1.31	1.38	1.39	1.39	1.37	1.20
1.0	1.31	1.34	1.36	1.41	1.42	1.40	1.39	1.37	1.16
1.06	1.34	1.37	1.39	1.43	1.44	1.38	1.39	1.36	1.09
1.07	1.35	1.37	1.38	1.40	1.37	1.37	1.36	1.33	1.04
1.09	1.35	1.37	1.38	1.40	1.37	1.32	1.30	1.27	.98
1.14	1.34	1.35	1.36	1.36	1.32	1.26	1.24	1.21	.94
1.20	1.33	1.34	1.34	1.34	1.30	1.23	1.21	1.18	.92
1.20	1.22	1.16	1.16	1.12	1.11	.99	1.0	.96	.75

Source | .04 | 1.15

FIG VI - 5 MH-1A CORE 3A (RODS IN)

RADIAL POWER DISTRIBUTION FOR CENTRAL
FUEL ASSEMBLY

TABLE XXXIII

Core 3A Peaking Factors

Radial peaking factor:	1.92
Axial peaking factor:	1.96
Engineering factor:	1.073
Total factor:	4.04

E. Depletion and Lifetime

The depletion of Core 3A was analyzed using the same procedures detailed in Section V, C. and D. The number density of boron-10 was adjusted at the beginning of each time step to maintain k within approximately 2 percent of 1.0. Figure VI-6 presents the resulting Δk for each time step.

When each Δk is subtracted successively from the initial k_{excess} of 1.086, the result present in Figure VI-7 (marked "k_{eff} summation") is obtained. From this curve, one concludes that the end of life condition is attained at a burn-up of 301 full power days, based on the k_{eff} summation technique (see Section V, C.)

The k_{eff} summation technique gives a value of k_{excess} = 1.00016 at 300 full power days. On the other hand, when a rods-out k calculation is performed at 300 full power days, one obtains k_{excess} = 1.01644. This latter value is to be taken as the true one since it is not based on a series of cumulative calculations, but is an independent k calculation. In addition, rods-out calculations made for the 350 and 400 full power day points yielded k_{excess} values of 1.00782 and 0.999204 respectively (labelled "explicit rods-out" in Figure VI-7). From these three values it is concluded that the true end of life of the core occurs at 395 full power days.

Some explanation is warranted of the difference between the end of life datum obtained by the k_{eff} summation technique and by the explicit rods-out calculations. The discrepancy in the k_{eff} summation technique arises from the discrete nature of the time steps utilized in the depletion. A simple, hypothetical depletion will serve as an example. Say a core has a BOL k_{excess} value of 1.010. Two time steps, 0-100 days and 100-200 days, are chosen for the analysis. Using the

82

FIG VI-6 MH-1A CORE 3A DEPLETION
k_{eff} VS. BURN-UP
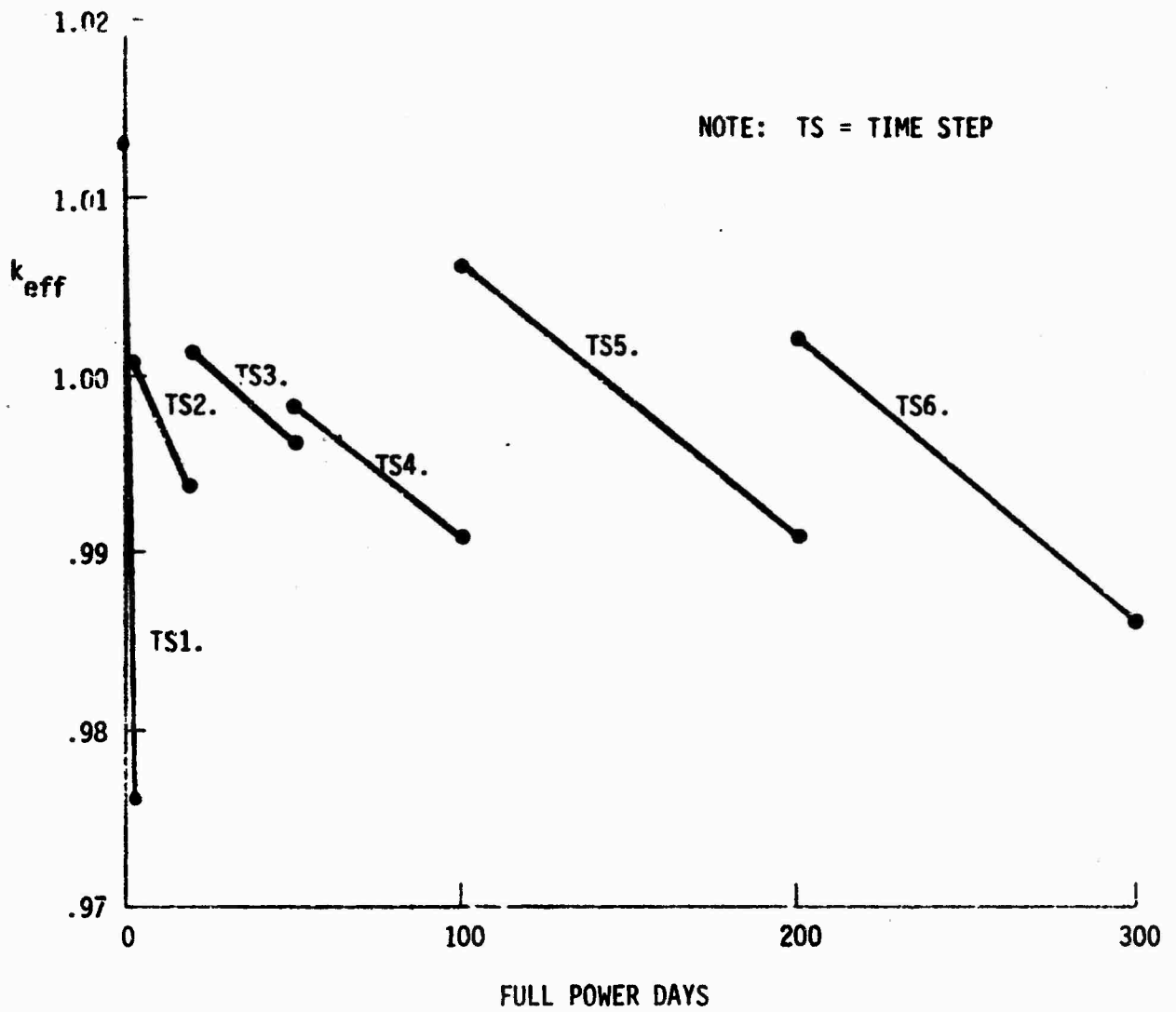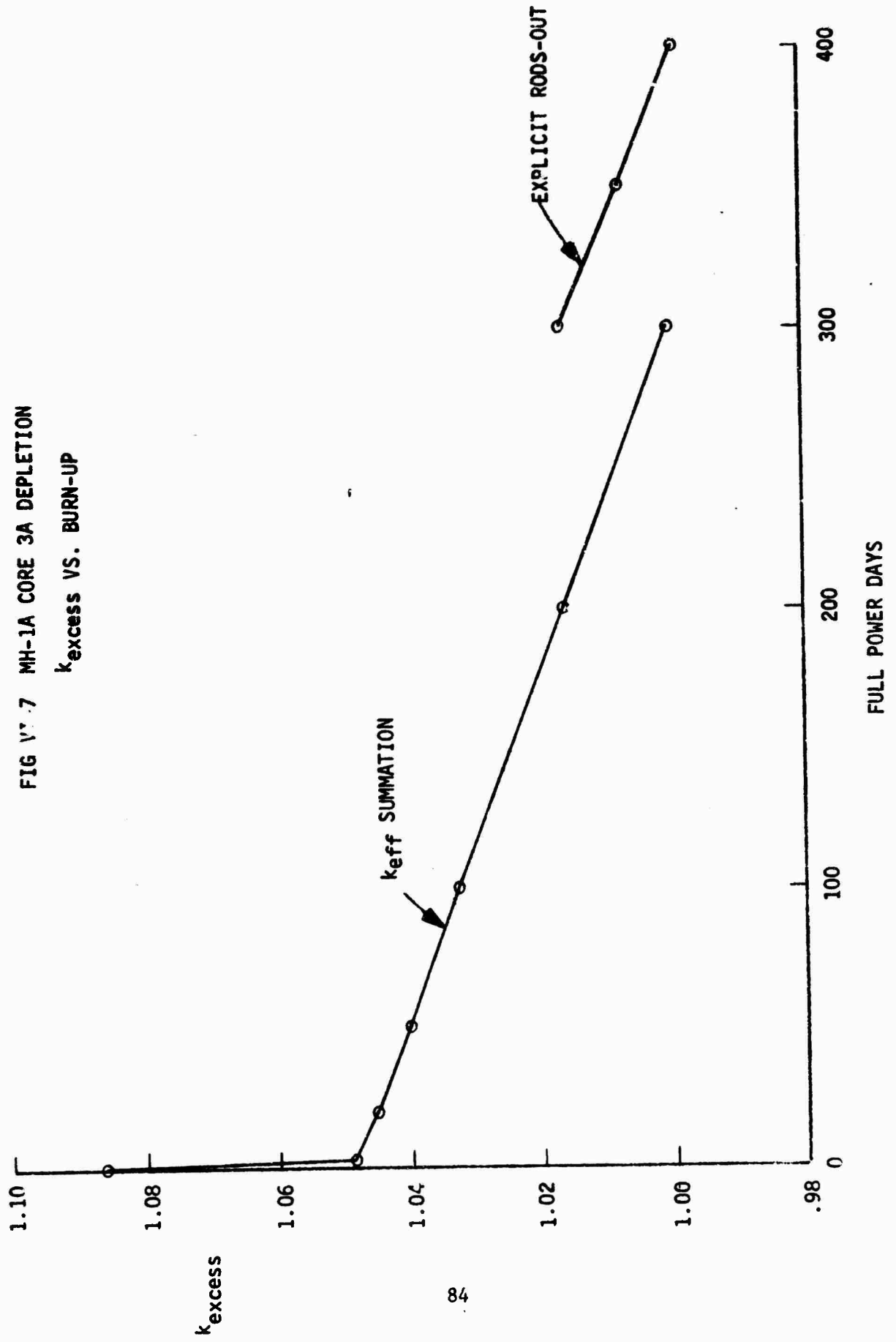
NOTE: TS = TIME STEP

83

FIG V.7 MH-1A CORE 3A DEPLETION
k_{excess} VS. BURN-UP

cross-section set for the first time step (cross-sections found for the 0 days case), say that the Δk found is 0.010. It is concluded that the core life-time is precisely 100 days. Now, if a rods-out calculation is performed for the 100 days point, the 100-200 day cross-section set will be used (since the cross-sections are always identified with the beginning of the time step). This calculation may give, say, $k=1.0005$ which contradicts the $k = 1.0$ expected from the k_{eff} summation calculation. The discrepancy between the two k values is due solely to the spectrum differences inherent in the two different cross-sections sets.

Thus it is concluded that the discrete nature of the time steps (i.e., the cross-sections do not vary continuously with time but change discontinuously with the definition of the time step interval) causes discrepancies in the k_{eff} summation technique. This technique may be trusted to indicate the trend that k_{excess} takes as burn-up proceeds; however, the true k_{excess} values, as they approach 1.0 must be explicitly found to determine the true end of life datum. In the above case of Core 3A at the 300 day point, an average contribution of 0.003256 to k for each time step, due to the spectral effects, would contribute the total discrepancy observed at 300 full power days.

The asymmetry error (see Section V, D.) may again be taken as the maximum uncertainty in determining the end of life datum -- in this case it is $\pm$ 15 days. Thus, the life-time of Core 3A is found to be:

395 $\pm$ full power days.

VII. FURTHER DETAILS OF COMPUTER CODES USED

A. LEOPARD

The LEOPARD code and its input procedures are discussed in Reference 1 and the supplement on its revision in August 1968. Familiarization with the latter is necessary to run the code correctly.

Several miscellaneous comments are necessary to complement the information in Reference 1. First, in running successive cases at different temperatures utilizing the change case option, one must re-enter the composition description input each time. Second, an end card with any real number (noninteger) greater than zero, punched anywhere in columns 73-80, must be added to the end of the LEOPARD input deck, otherwise an end-of-file error message will result. And third, if a "1" is punched in column 24 of the options card (the card immediately following the title card), the program will punch out the cross-section library for use in an associated TURBO* calculation. It should be noted that the "DEC 1015" card is punched last and must be properly repositioned within the resulting TURBO* deck.

B. LEOPROD

The LEOPROD input deck is almost identical to the LEOPARD input deck except that some additional cards are required. Two cards are added after the usual title card. The first card consists of five fields of four columns each. In the first field an integer IFLAG is to be punched in column 4. This integer determines what calculational option is being chosen as detailed in Table XXXIV.

TABLE XXXIV

IFLAG Options

Value of IFLAG	Case Considered
1	Purely absorbing B-SS absorber slab.
2	Other slab compositions with no scattering.
3	Tubular absorber rods in cruciform rod.
4	Absorber slab with scattering present.
5	No calculation done, only an explanation of the input required is printed.

86

The remaining four fields each contain one integer identifying up to four other elements which may be present in the absorber besides boron-10. Table XXXV lists the identifying integer associated with each element. If less than four other elements are required, the remaining fields should each have a "25" entered. Do not leave a field completely blank; all integers should be right justified within their field (e.g., otherwise "6" may be read as "60", etc.).

TABLE XXXV

Element Identification for LEOPROD

Element	Integer	Element	Integer	Element	Integer
hydrogen	1	manganese	9	F.P.	17
oxygen	2	U-235	10	B-10	18
zirconium	3	U-236	11	D	19
carbon	4	U-238	12	Th-232	20
iron	5	U-239	13	Pr-233	21
nickel	6	Pu-240	14	U-234	22
aluminum	7	Pu-241	15	U-233	23
chromium	8	Sm-149	16	U-234	24
				Nothing	25

The second card after the title card specifies the number densities in and the dimension of the absorber region. This card consists of six fields of twelve columns. The first field is used to input the boron-10 number density (in atoms per cubic angstrom). The second field is for one-half the mean chord length in the absorber region. For a slab this is equal to its thickness; for a rod this is equal to its radius. In any other geometry, it is equal to twice the absorber volume, divided by the absorber surface area. The remaining four fields are used to enter the number densities of the four other elements, besides boron-10, in the absorber. They should be entered in the same order that they are identified on the previous card. Blank fields are interpreted as zeroes and allowed. If these two LEOPROD data cards are inadvertently reversed in order, an "illegal decimal" error message will be printed.

The remaining, usual LEOPARD data cards follow these two LEOPROD cards. At the end of these, comes the LEOPROD end card. This card has one field made up of the first twelve columns. If "0.0" is punched anywhere in this field, the job stops at the end of the current

87

case. If "1.0" is punched in this field, the job continues with a
LEOPROD calculation for the next case using the same cell spectrum.
For this next case, only the title and the two LEOPROD input cards
which follow it need be input (plus an appropriate LEOPROD end card).
If "2.0" is punched in this field, the next case is considered as a
completely new calculation with a new cell spectrum being calculated.
For this case, the entire LEOPROD - LEOPARD input deck needs to be
input anew. The purpose of these options is to give flexibility in
making multiple runs. Unlike LEOPARD, LEOPROD does not have a
depletion option.

There remains one LEOPROD input card required in a special case
(Ref. 14). If the calculation of constants for a tube-filled cruci-
form control rod (see Fig VII-1) is desired, i.e., IFLAG is 3, an
additional data card is required. This card just precedes the LEOPROD
end card and consists of two fields of twelve columns. The first
field consists of the tube clad thickness, the second field consists
of the tube outer radius. Any units are allowed as long as these two
quantities are consistent. For this option, the dimension entry on
the second LEOPROD card (the number density card) should be the tube
outer diameter in centimeter units. If the IFLAG = 3 option is not
specified, this data card is absent.

TABLE XXXVl

LEOPROD Compared to LEOPARD

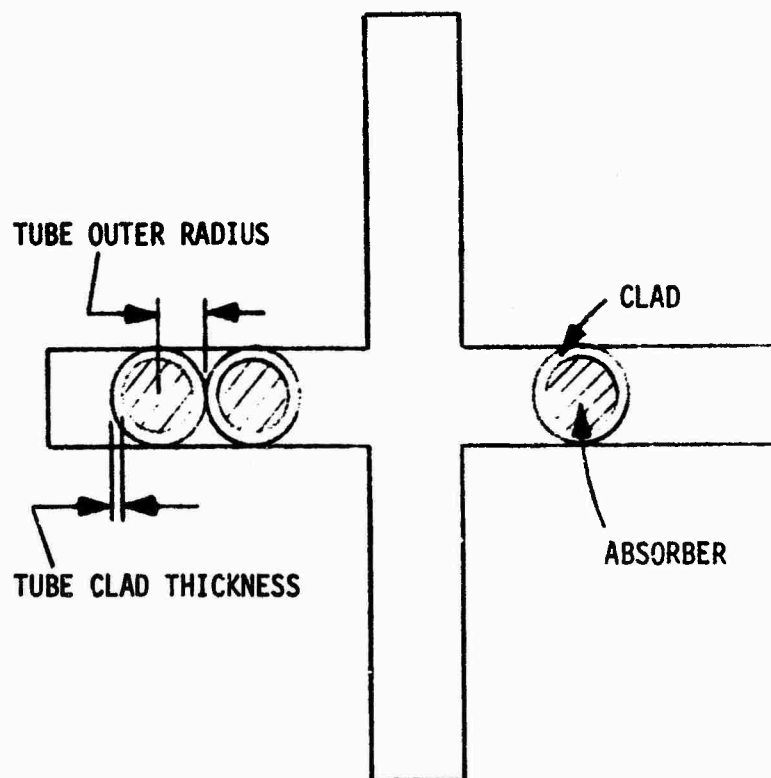| Altered Subroutines	Unchanged Subroutines
INPUT	HEADER
THERMAL	MOVEAA
ED34	ACCUM1
THREE	VCL
OUTPUT	INGR
	QD
	MUFT
	SLOW
	RESINT
Unused Subroutines	**New Subroutines**
BTEST	BRANCH
WORKS	TUBE1
AKTVAN	XPLAIN
COMPOS	TABLE
BURN	BLOCK
WYE	
MASSED	

FIG VII-1 TUBE FILLED CRUCIFORM CONTROL
           ROD GEOMETRY

C. TURBO*

If the TURBO* cross-section library is punched out by the LEOPARD modification option, several measures must be taken. First, any blank columns must have zeroes entered in them for acceptance in TURBO*. Second, the "+" sign is omitted from the E format numbers punched out and must be explicitly entered, where missing, for acceptance in TURBO*. Third, if additional cards are added to the cross-section deck, an appropriate change must be made in the final number on the "DEC 1015" card.

90

REFERENCES

1. WCAP-3269-26, "LEOPARD-A Spectrum Dependent Non-Spatial Depletion Code for the IBM-7094", R.F. Barry, September 1963. Revised August 1968 for the IBM-360.

2. "Interim Engineering Support Study: MH-1A First Shuffle Core Nuclear Analysis", 15 August 1969.

3. ED-6916, "MH-1A Steady State and Transient Thermal Hydraulic Design Analysis", C.A. Myers et al., July 1969.

4. WAPD-218, "A Theoretical Method for Determining the Worth of Control Rods," A.F. Henry, August 1959.

5. "Advanced Reactor Physics," A.F. Henry, M.I.T. Course Notes, Fall 1968.

6. NUS-407, "MH-1A Second Generation Core Design Report, Nuclear Analysis", E.E. Rilat et al., October 1967.

7. NUS-576, "Type II Core Design for the MH-1A", October 1969.

8. WCAP-6059, "TURBO* - A Two Dimensional Few-Group Depletion Code for the IBM-7090", S.M. Hendley et al., March 1964.

9. A.M. Weinberg, E.P. Wigner, The Physical Theory of Neutron Chain Reactors, 1958.

10. ED-6923, "MH-1A Refueling, 17-25 October 1969", C.F. Sears, December 1969.

11. J. R. Lamarsh, Introduction to Nuclear Reactor Theory, 1966.

12. ED-7002, "MH-1A Core Physics Test Report", C.F. Sears and M.V. Gregory, 1970.

13. MND-3238, "MH-1A Final Design Report, Nuclear Analysis", W.P. Kutz, 1965.

14. M. Michelini, Neutron Transmission Probabilities Across Control Blades Filled with Round Tubes: Formulation and Accuracy", Nuclear Science and Engineering, Nov 1970.

15. TID-7030, Naval Reactors Handbook, Vol. I, A. Radkowsky ed., 1964.

91

APPENDIX A

CONTROL ROD CONSTRUCTION

Reactor control is provided by 12 cruciform-shaped control rods located between the fuel elements. The core complement consists of 12 identical control rods, with the control material boronated stainless steel, a material that has been used extensively throughout the industry for similar control rods. The follower sections of the control rods consist of welded cruciform-shaped structures of stainless steel. These cruciform control rods are suspended from top-mounted rack and pinion drives, and ride within channels formed by the fuel elements and slots in the core support structure.

TABLE I

Description of Type I Modified Control Rods

Control material	2.25 w/o enriched 92% B^{10} in austenitic stainless steel
Length of borated stainless steel, in.	36.75
Follower	Type 347 stainless steel.
Length follower, in.	41.9
Width of blade, in.	10.8
Poison thickness, in.	.250
Side cladding, in.	0.050 Type 347 stainless steel
Construction	Plates within cladding with solid follower section.

Each control rod with end fittings is approximately 8 feet in length and weighs approximately 200 pounds. During scram, the control rods will be subjected to an acceleration of less than 100 g. The handling fixtures (fixture at top of rod), the clad, and the fasteners have been designed to sustain this dynamic load throughout core life.

The poison material is sandwiched between the stainless clad, which acts as a structural member and transfers the loads from the handling fixture to the follower section. No strength requirements are imposed upon the contained poison plates.

A-1

As shown in Table I, the control material is austenitic stainless steel containing 2.25 w/o of 92 percent boron. The poison plates are 36.75 inches long and align with the active fuel length after the control rods are attached to the drive mechanisms.

The poison plates are manufactured by making a single casting; cogging or rough rolling of the billet for break-down and then cutting the billet into slabs. The slabs are rolled to an appropriate thickness and finish ground. The master plates are cut transversly into widths to use as poison plate material. The end of each control rod plate is trimmed, and three samples are taken for chemistry and boron control evaluation.

Chemical sampling showed that the boron content specification was met within a 95 percent confidence that 95 percent of all material over the entire volume of the poison plates, and that the maximum local deviation of boron content was within plus or minus 5 percent the average.

Each poison plate is assembled to its cladding components and line drilled. After disassembly and cleaning, final assembly is made with screw fasteners which are then tack welded to the cladding. A threaded boss is welded to the top cruciform filler piece. A handling fixture stud is threaded to engage with, and fasten to, this boss. After adjusting the total length, the fixture stud is pinned and plug welded.

After assembly and welding have been completed, each of the control rods are measured for conformance to the envelope requirements of drawing No. 500050. If straightening is required, a maximum of .025 inch is allowed. Straightening of individual pieces before assembly is allowed provided the final operation is an annealing operation. This requirement is to assure that the material in the control rods, when inserted in the reactor, are in the "relaxed" condition.

When disconnected from the control rod drive mechanism, the base of the control rods rest on the core barrel orifice plate (at the same time, they shadow the entire fuel length of 36 inches).

When connected to the control rod drive mechanism, the rod is raised a nominal 0.75 inch above the orifice plate, and under scram conditions, the control rods do not strike the orifice plate.

A description of the differences in design between the original control rods fabricated by Martin Co. and the rods designated Type I-Modified and manufactured by NUCOM, is contained in the remainder of this appendix.

To increase the reliability and shorten the lead time in procurement, a review was made of the design of the MH-1A Type 1 control rods. Upon completion of the review, several changes were made in the fabricated package. One set of changes affected the nuclear properties of the control rod and the other group reflected detail design changes for increased reliability and decreased cost.

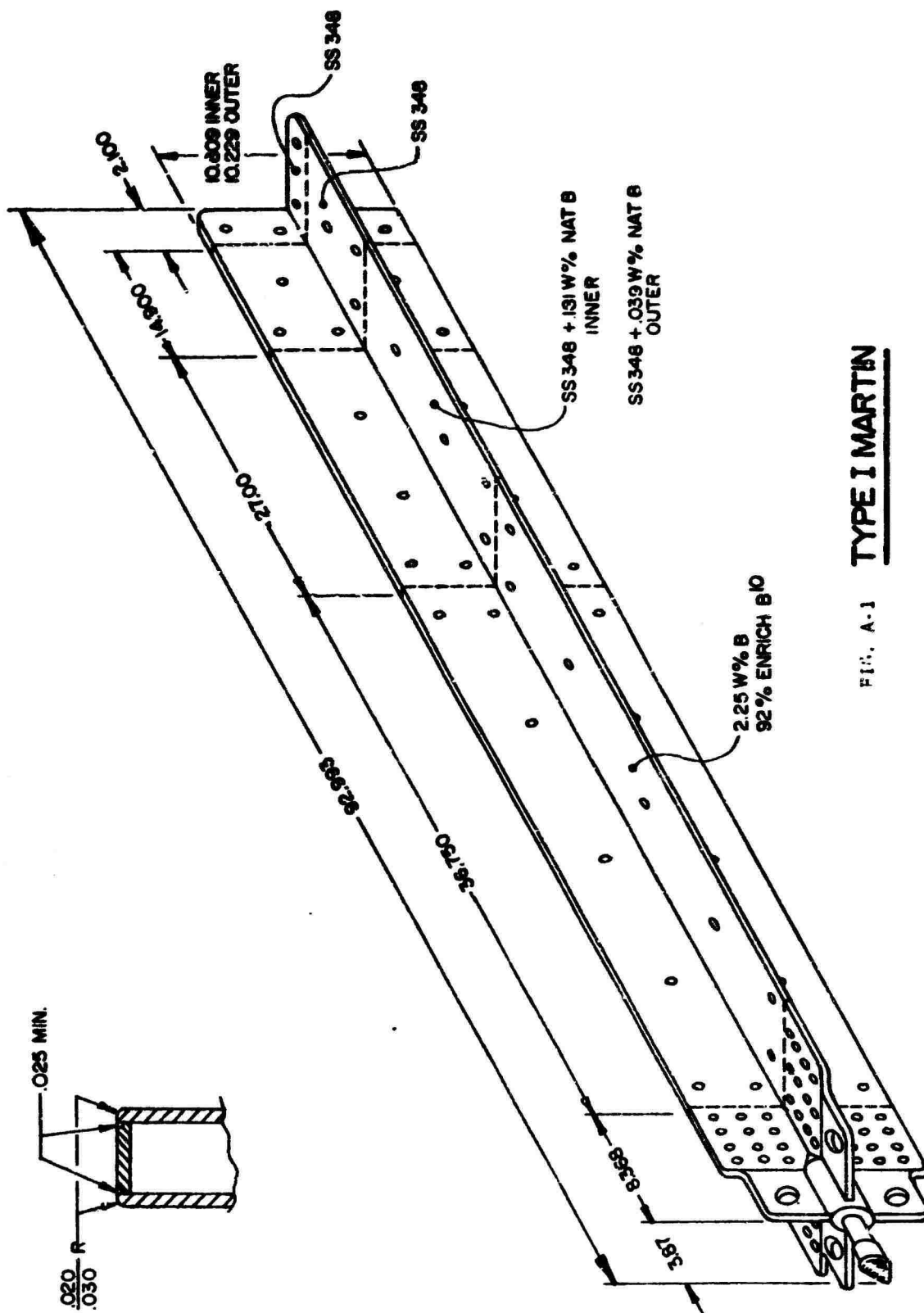The detail changes which affected the nuclear properties are:

1. A change in the blade widths from two sizes, (i.e., the original control rods required 10.229 inches for the outer group of rods and 10.809 inches for the inner group of rods) to one size in the present construction for all 12 rods in the reactor to 10.809 inches.

2. The reduction of three different alloys of stainless steel with boron to a single alloy of stainless steel with boron (i.e., the original requirement of S.S. with 2.25 w/o boron enriched 92 percent B^{10} in the absorber section and S.S. with .181 w/o natural boron in follower section of the inner control rods and S.S. with .039 w/o natural boron in the follower section of the outer control rods was changed in present procurement to 2.2 w/o enriched 92 percent B^{10} in the absorber section and to standard stainless steel in the follower sections of both inner and outer control rods).

The design changes which reflect increased reliability and fabricability are:

1. The cladding was reduced in length from 89-1/4 inches to 50-1/4 inches.

2. The blade tip edge of the borated stainless steel was chamfered to preclude any boron pickup during the edge clad weld.

3. The follower assembly was made as a rigid welded structure, rather than plates held together by the cladding.

4. A minimum ferrite content was specified and maintained in the edge clad welds.

5. The edge clad weld was specified as a full penetration to a .035 inch minimum weld rather than a .015-.035 inch penetration weld.
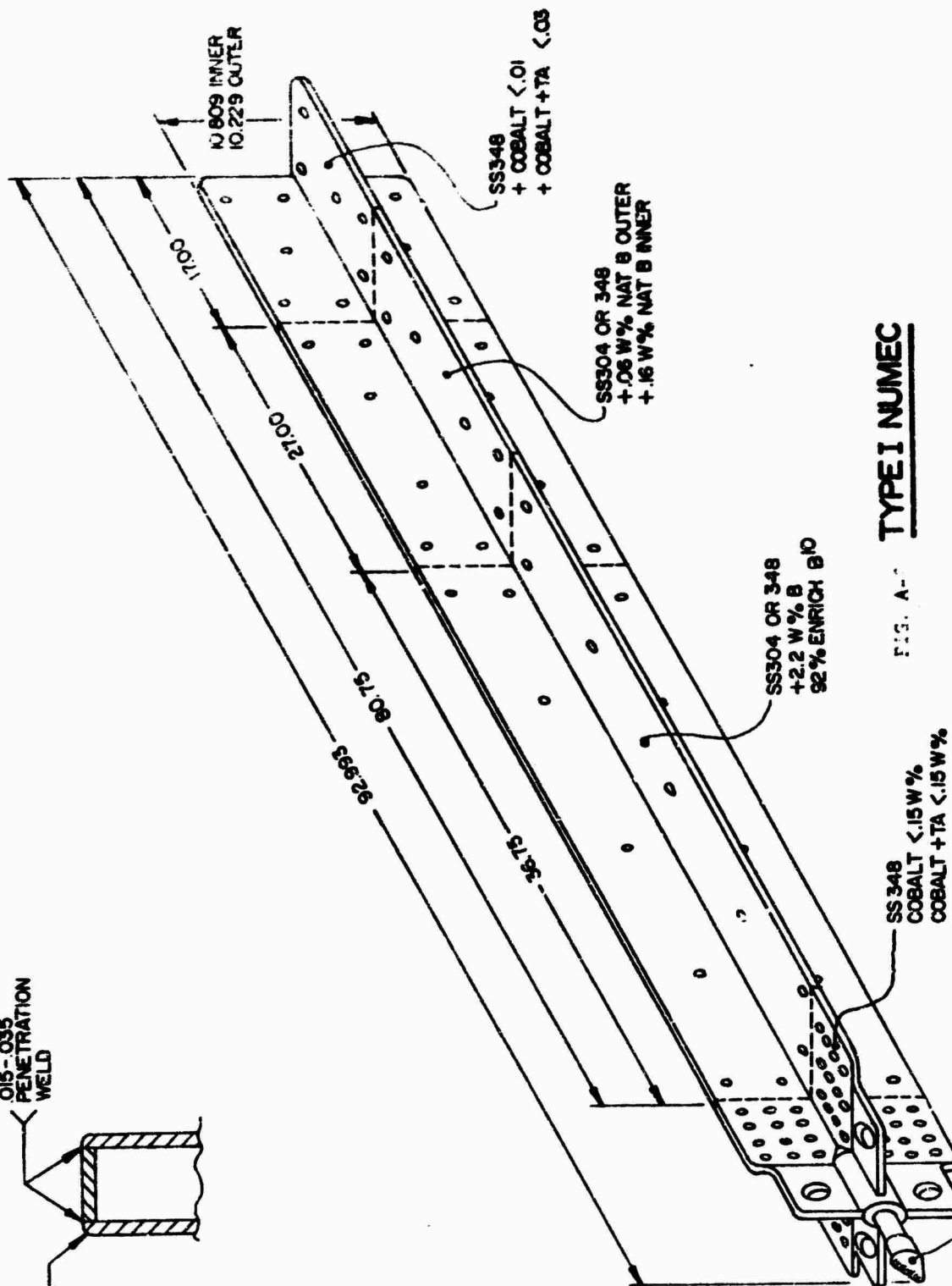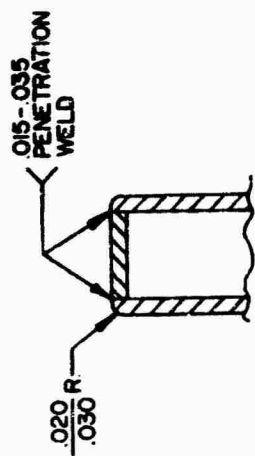
A-3

6. Addition of filler metal rod with controlled ferrite was specified in tack welding the connectors to the cladding, rather than a fusion weld with no filler metal allowed.

7. A .003 inch gap was specified between the edge clad and the borated stainless steel absorber, rather than having the edge clad flush against the borated stainless steel.

The number of connectors transferring the loads between the cladding and other structures was not reduced, but was rearranged.

FIG. A-1   TYPE I MARTIN

SS 348
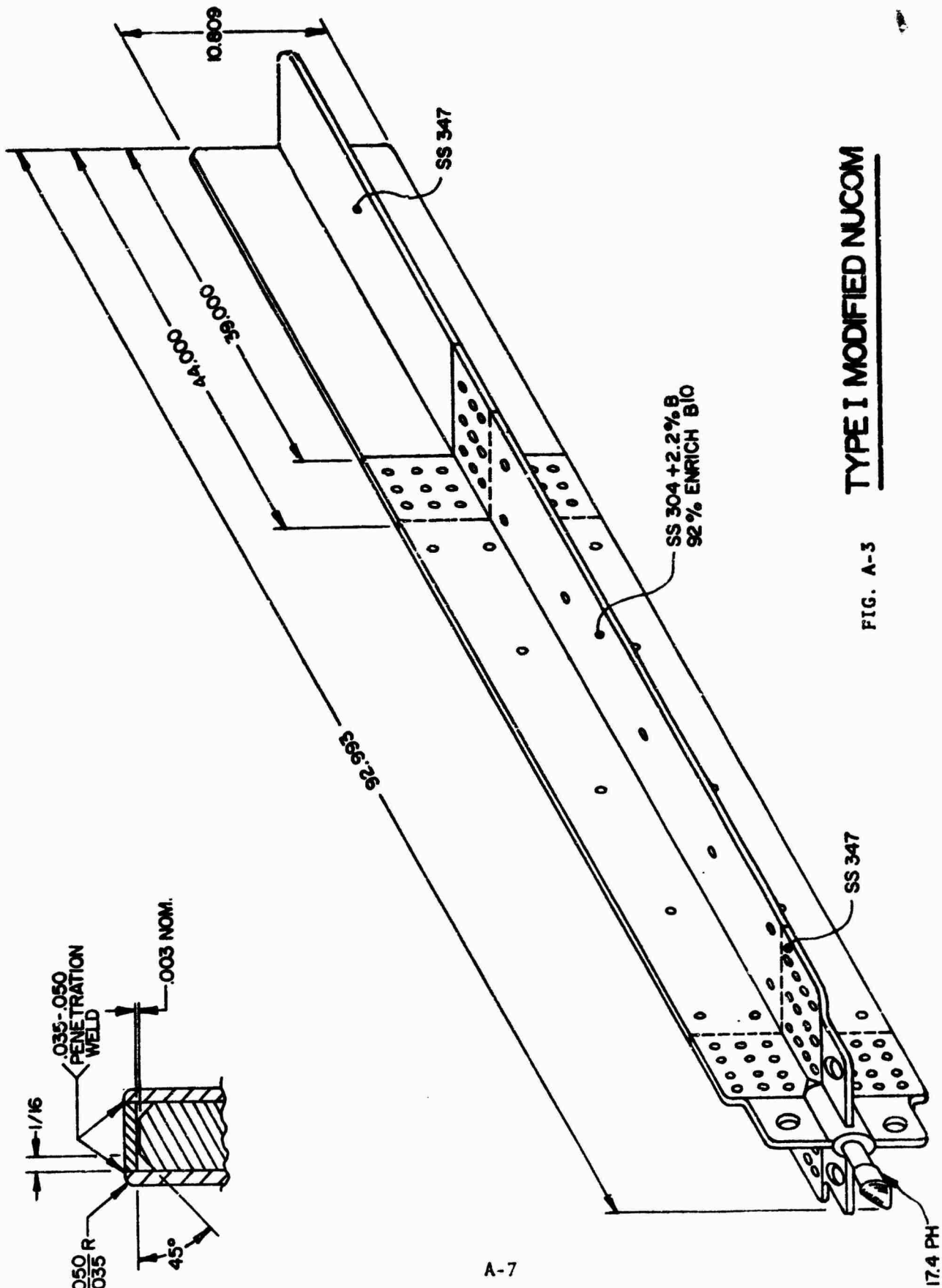
SS 348

10.609 INNER
10.229 OUTER

2.100

14.900

27.00

96.750

89.990

SS 348 + .131 W% NAT B INNER

SS 348 + .039 W% NAT B OUTER

2.25 W% B
92% ENRICH B10

8.368

3.87

.025 MIN.

.020
.030 R

RE-1634

A-5

TYPE I NUMEC

FIG. A-5

A-6

RE-1836

TYPE I MODIFIED NUCOM

FIG. A-3

SS 347

SS 304 + 2.2% B
92% ENRICH B10

SS 347

17.4 PH

10.909

78.000

44.000

92.993

.035-.050
PENETRATION
WELD

.003 NOM.

1/16

.050 R
.035

45°

A-7

RE-1636

DOCUMENT CONTROL DATA - R & D

(Security classification of title, body of abstract and indexing annotation must be entered when the overall report is classified)

1. ORIGINATING ACTIVITY (Corporate author)	2a. REPORT SECURITY CLASSIFICATION
Engineering Division U. S. Army Engineer Reactors Group Fort Belvoir, Virginia	UNCLASSIFIED
	2b. GROUP

3. REPORT TITLE

The Theoretical Nuclear Analysis of the MH-1A: Cores 2 and 3

4. DESCRIPTIVE NOTES (Type of report and inclusive dates)

Final Report

5. AUTHOR(S) (First name, middle initial, last name)

Gregory, Michael V.   Lillie, Richard A.
Iyer, Shrinivas S.   Henry, C. Daniel

6. REPORT DATE	7a. TOTAL NO. OF PAGES	7b. NO. OF REFS
	98	15
8a. CONTRACT OR GRANT NO. IN-HOUSE	9a. ORIGINATOR'S REPORT NUMBER(S)	
b. PROJECT NO.	ED-7102	
c.	9b. OTHER REPORT NO(S) (Any other numbers that may be assigned this report)	
d.		

10. DISTRIBUTION STATEMENT

Qualified requesters may obtain copies of this report from DDC.

11. SUPPLEMENTARY NOTES	12. SPONSORING MILITARY ACTIVITY
	U. S. Army Engineer Reactors Group Corps of Engineers

13. ABSTRACT

This report presents the methods and results of the theoretical analysis of the nuclear properties of MH-1A Cores 2 and 3. The basic physical parameters are obtained by use of two cross-section codes, LEOPARD and LEOPROD, an X-Y geometry depletion code TURBO*, plus a Z-axial calculation using the CNCR-2 code together with the HOMOG and PEAK processor codes. The theory, results, and input details of the LEOPROD blackness theory code giving absorber region constants are considered in some detail.

DD FORM **1473** REPLACES DD FORM 1473, 1 JAN 64, WHICH IS
NOV 65 OBSOLETE FOR ARMY USE.

D—30,074—8t Belvoir